immunoprecipitation buffer (50 mM Tris-HCl pH 7.5, 100 mM NaCl, 0.5% NP-40, 200 μM PMSF, 50 μM VO_4, 2 μg/ml Aprotinin, 5 μg/ml Leupeptin, 1 μg/ml Pepstatin A). For immunoprecipitation assay, cell lysate or wheat germ cell extract generating full-length HPIV3-HN was incubated with the individual MAb (hybridoma supernatant), preclearing overnight using proteinA/G sepharose beads, for 2 h at 4°C. After washing three times with immunoprecipitation buffer, immunocomplexes were eluted from the beads with 2x SDS sample buffer. Then, the bound protein was analyzed by immnoblotting.

IMMUNOFLUORESCENCE

HeLa cells were grown on coverslips for 24 h and the cells were infected with HPIV3 (MOI = 100); mock-infected cells served as the control. At 48 h post-infection, the cells were washed with PBS before fixation with 3% formalin in PBS at room temperature for 15 min. Cells were washed twice with PBS for 5 min followed by 100% methanol for 10 min at −20°C. Cells were permeabilized with PBS containing 0.05% Triton X-100 for 10 min at room temperature. The cells were incubated with individual primary antibodies for 1 h at room temperature. After being washed twice with PBS, the cells were incubated with secondary antibodies for 1 h at room temperature. The nucleus was counterstained with 4′,6-diamidino-2-phenylindole (DAPI). Microscopic imaging was performed with an FV1000-D confocal laser scanning microscope (Olympus, Tokyo, Japan) equipped with a 60x oil-immersion objective.

FLOW CYTOMETRY

HeLa cells were seeded in 6-well plates at a concentration of 2×10^5 per well 24 h before infection, and the cells were washed with medium containing 0.0001% trypsin and infected with HPIV3 (MOI = 100); mock-infected cells were used as a control. At 4 days post-infection, cells were harvested in PBS containing 5 mM EDTA and washed twice with PBS. The cells were then incubated with either MAbs (hybridoma supernatant; 5X dilution) or non-immunized hybridoma supernatant in PBS containing 2% Blocking One (NACALAI TESQUE, INC., Kyoto, Japan) for 1 h at room temperature. After being washed twice with PBS, the cells were incubated with phycoerythrin (PE)-conjugated anti-mouse IgG antibodies (Beckman Coulter, Fullerton, CA, USA) for 1 h at room temperature. Flow cytometric analysis of the cells (10,000 cells per sample) was performed on a FACScanto II instrument (BD Biosciences, San Jose, CA, USA).

EPITOPE MAPPING AND SPECIFICITY OF MAbs USING ALPHASCREEN ASSAY

The AlphaScreen assay was performed using 384-well ProxiPlates (PerkinElmer, Boston, MA, USA). Biotinylated virus proteins or GST (negative control) were incubated with a 40-fold dilution of MAbs (hybridoma supernatant) in 15 μl of binding mixture containing reaction buffer (100 mM Tris-HCl, pH 7.5, 1 mg/ml BSA, 0.01% Tween-20) at 26°C for 30 min. Then, combine 10 μl of the detection mixture containing 0.1 μl protein G-conjugated acceptor beads and 0.1 μl streptavidin-coated donor beads (AlphaScreen IgG detection kit, PerkinElmer) in reaction buffer were incubated at 26°C for 1 h. Antigen-antibody interactions were analyzed using an Envision microplate reader (PerkinElmer).

PROTEOMIC ANALYSIS

Cell lysate from HPIV3-infected or mock-infected HeLa cells were immunoprecipitated with #21 MAb. The binding proteins were separated by SDS-PAGE and transferred to PVDF membranes. For LC-MS/MS analysis, the membranes digested with trypsin. LC-MS/MS analysis was performed using a TripleTOF MS (TripleTOF 5600 system, AB SCIEX, Foster City, CA, USA) and the Analyst version 1.6 TF (AB SCIEX) coupled to an DiNa-AP (KYA Technologies, Tokyo, Japan). Prior to injection into the mass spectrometer, the tryptic digests were filtered through a Ultrafree-MC, GV 0.22 μm filter (Millipore), then loaded onto a reverse phase pre-column (HiQ sil C18W-3, 500 μm id × 1 mm, KYA Technologies) and resolved on a nanoscale HiQ sil C18W-3 (100 μm id × 10 cm; KYA Technologies) at a flow rate of 200 nL/min with a gradient of acetonitrile/0.1% (v/v) formic acid. Peptides were separated using a 30 min gradient from 5 to 100% solvent B [0.1% (v/v) formic acid/80% (v/v) acetonitrile]. Solvent A was 0.1 % (v/v) formic acid/2% (v/v) acetonitrile. The obtained MS and tandem-MS data were searched against the human protein sequences in the Swiss-Prot database (version Jan 2013, 20233sequences) using the Protein Pilot software 4.5 (AB SCIEX).

RESULTS

PRODUCTION OF MAbs

In our current study, we attempted to produce the full-length HPIV3-HN by the wheat cell-free production system (**Figure 1A**). Complementary DNA encoding HPIV3-HN open-reading frame was sub-cloned into pEU-His, the expression vector designed specifically for the wheat germ cell-free system for expressing His-tagged protein. Consequently, His-tagged HPIV3-HN protein was synthesized by this procedure in a large scale. Since HPIV3-HN exhibited high insolubility in regular buffer, the protein was suspended in the buffer including 8 M urea. This suspended His-tagged HPIV3-HN was further purified using Ni-sepharose followed by the elusion with imidazole. Balb/c mice were then immunized with purified full-length HPIV3-HN protein. After 4 weeks, splenocytes were isolated and hybridomas were created (**Figure 1A**). Finally, 36 stable hybridomas were obtained and designated #1 to #36. The resulting hybridomas were screened by ELISA with plates coated with HPIV3-HN protein conjugated with BSA. Of the 36 hybridoma clones established, seven clones (#4, #5, #7, #10, #14, #21, #23) exhibited relatively high absorbances (**Figure 1B**). Titration analyses with diluted hybridoma supernatants or antigenic HN protein revealed that these seven antibodies had higher specificities and intensities than control hybridoma supernatants (**Figure 1C**). These seven hybridomas were processed for further characterization.

IMMUNOBLOTTING ANALYSES OF MAbs

We next tested the MAbs in immunoblotting analysis. First, recombinant HPIV3-HN protein was separated by SDS-PAGE followed by immunoblotting with MAbs isolated from the seven

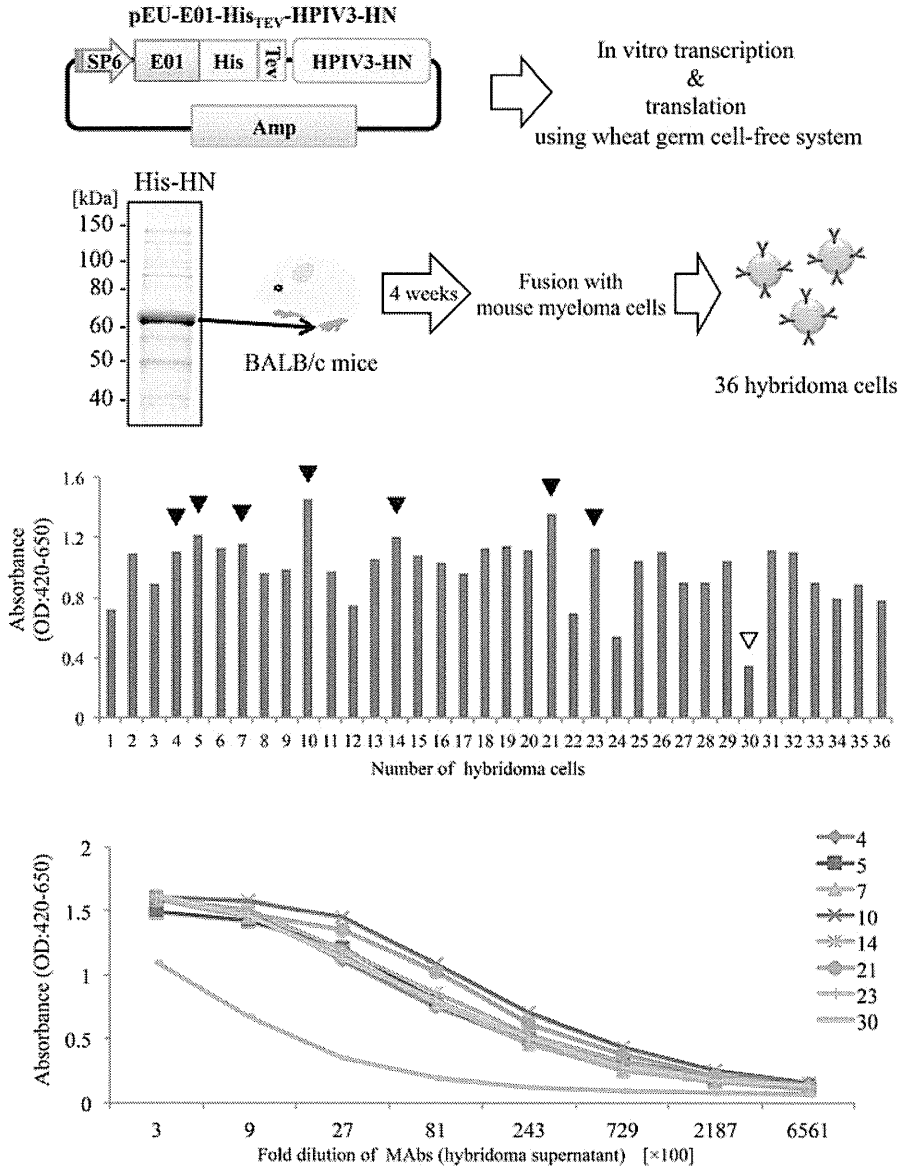

FIGURE 1 | Production of hybridoma cells generating anti-HPIV3-HN antibodies. (A) Schematic diagram of hybridoma cells production generating anti-HPIV3-HN monoclonal antibody (MAb). The recombinant Histidine-tagged recombinant HPIV3-HN (His-HN) protein was produced by wheat germ cell-free system and then purified by nickel-chelated sepharose beads in the presence of 8 M urea. The purified protein was separated by SDS-PAGE and visualized by CBB-staining. Purified His-HN protein was injected into the footpad of Balb/c mice. After 4 weeks, immunized mouse splenocytes were fused with myeloma cells and then 36 hybridoma cells were established. SP6, SP6 promoter sequence; E01, translation enhancer sequence; His, Histidine-tagged sequence; TEV; TEV protease recognized sequence. **(B,C)** The specificity of MAbs (hybridoma supernatant) evaluated by ELISA. The specificity of 36 MAbs in 2700-fold dilution was determined **(B)**. The black arrows indicate the selected MAbs while the white arrow depicts a selected clone as a negative control (clone no. #30). The selected eight MAbs were diluted at serial points and analyzed by ELISA **(C)**.

hybridomas. As shown in **Figure 2A**, all seven MAbs recognized a single band that corresponded to the recombinant protein. Next, immunoblotting analysis was performed with cell lysates from HeLa cells either infected- or mock-infected with HPIV3. The all seven MAbs detected a 63 kDa protein band that was consistent with the molecular mass of the HN protein (**Figure 2B**). No other bands were detected by the MAbs indicating that they specifically recognized HN.

IMMUNOFLUORESCENT ANALYSIS

We next performed an immunofluorescent (IF) analysis of HPIV3-infected HeLa cells with seven MAbs (**Figure 2C**). Three of the MAbs (#7, #21, and #23) exhibited prominent IF staining of the infected cells, while the other four MAbs had no detectable IF staining. The IF staining with the antibodies revealed that HN protein exhibited granular staining pattern throughout cytoplasm and plasma membrane in HPIV3-infected cells (**Figure 2D**), which

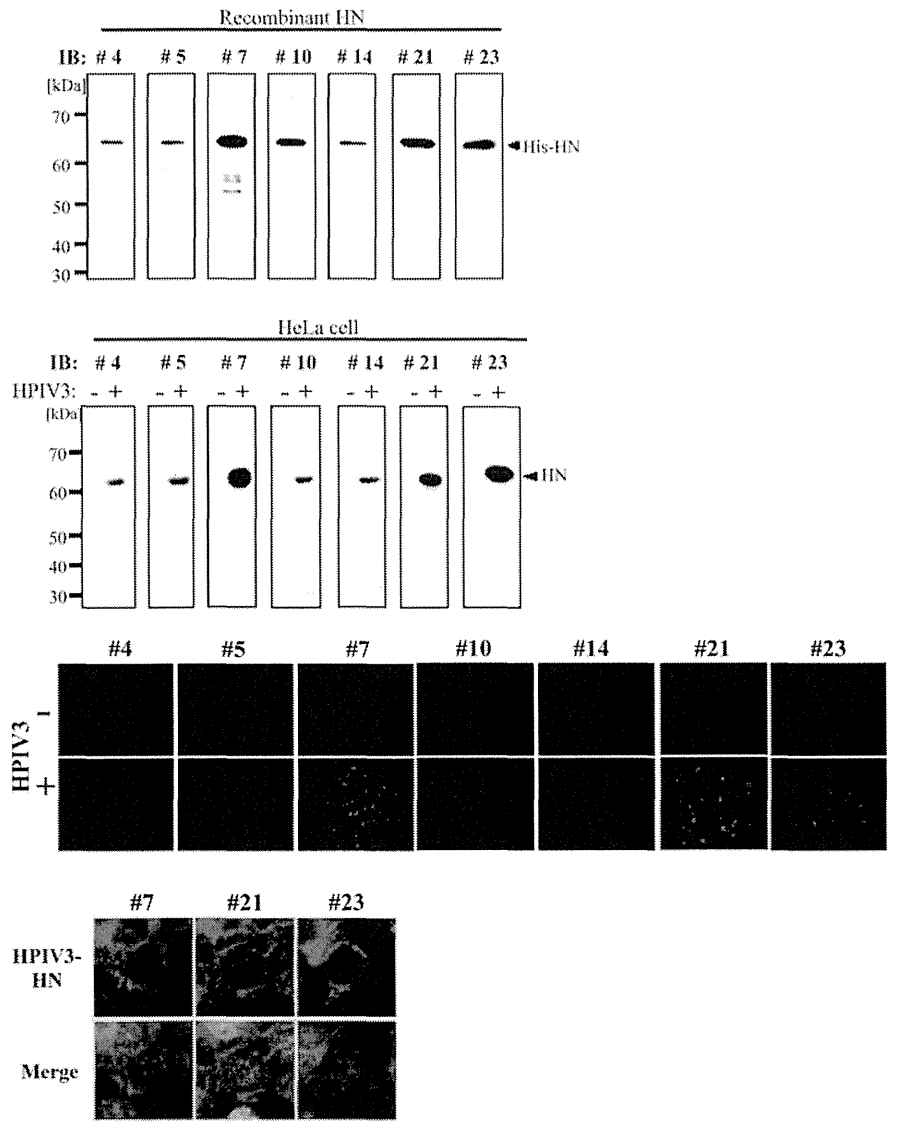

FIGURE 2 | Immunoblotting and immunofluorescent analysis. **(A,B)** Detection sensitivity of the MAbs for recombinant His-HN **(A)** or HPIV3-infected cell lysate **(B)**. Recombinant HPIV3-HN (100 ng) was separated using 12.5% SDS-gel and transferred to a PVDF membrane, followed by incubation with MAbs (hybridoma supernatants) at a 1:10 dilution **(A)**. HeLa cells were infected or mock-infected with HPIV3. After 48 h, cells were lysed with SDS-PAGE loading buffer. The total protein was separated in 12.5% SDS-gel and immunobloted with indicated MAbs **(B)**. **(C,D)** Immunofluoresent analysis of HN (red) in HPIV3-infected HeLa cells. HeLa cells were infected or mock-infected with HPIV3. After 48 h, cells were fixed, and then stained with MAbs (hybridoma supernatant; red) and DAPI (blue). Confocal microscopic analysis was performed at 40× **(C)** and at 600× magnifications **(D)**.

was consistent with previous studies (Ali and Nayak, 2000; Stone and Takimoto, 2013). The control mock-infected cells did not show any signals when stained with the antibodies (**Figure 2C**). We thus selected the three MAbs (#7, #21, and #23) for further characterization.

IMMUNOPRECIPITATION

We next examined whether these selected antibodies were useful in immunoprecipitation analysis. The wheat germ extract containing full-length HPIV3-HN with glutathione-*S*-transferase (GST) tag was incubated with protein A/G-coated sepharose beads (GE Helthcare) together with the three selected antibodies or non-immunized mouse IgG antibody. The precipitated samples were subjected to immunoblotting analysis with anti-GST antibody. The GST tagged HN protein was precipitated by all selected antibody (#7, #21, and #23) but not non-immunized IgG (**Figure 3A**).

FLOW CYTOMETRY ANALYSIS

We next addressed the usability of the antibodies #7, #21, and #23 in flow cytometry analysis. HeLa cells infected with HPIV3 were stained with the antibodies and then subjected to FACS analysis.

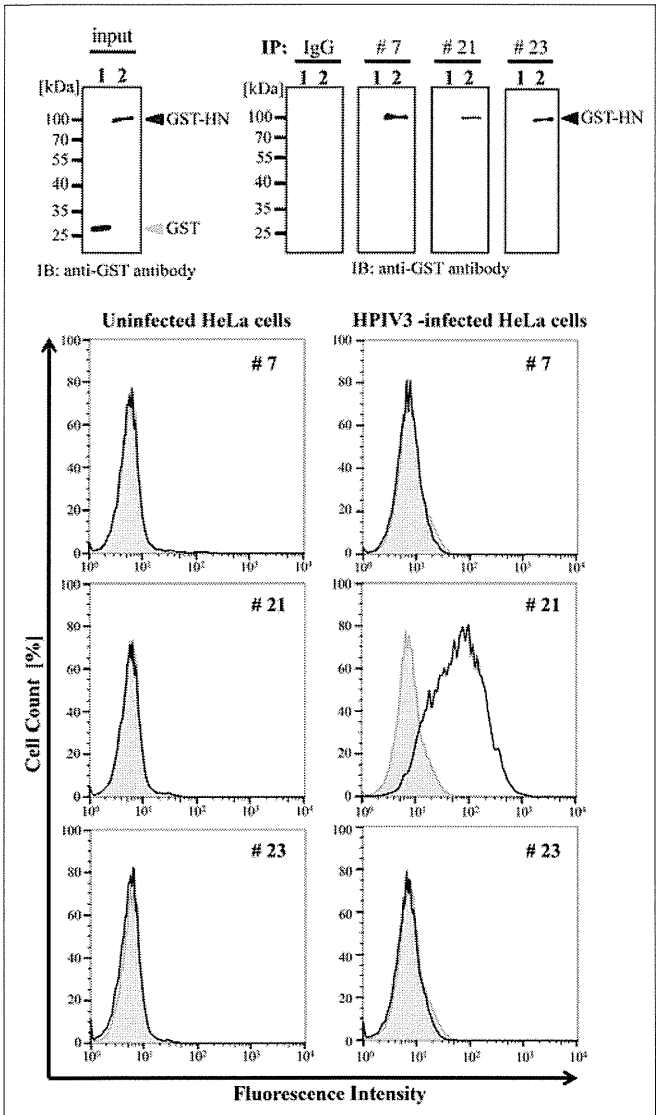

FIGURE 3 | Immunoprecipitation and flow cytometry assay. **(A)** Recombinant GST-HPIV3-HN or GST protein was immnoprecipitated with either #7, #21, #23 MAbs, or IgG (negative control), respectively. Then bound proteins were analyzed with immunoblotting using anti-GST antibody. **(B)** HPIV3-infected or uninfected HeLa cells were harvested at 4 days post-infection, followed by incubation with indicated MAbs. The cells were then fixed and stained with anti-mouse secondary antibody. The population of stained cells was calculated by flow cytometry. The shaded histogram shows negative hybridoma supernatant and the bold line shows specific MAbs.

Our results demonstrated that only #21 MAbs could specifically detect virus-infected cell populations, and distinguished between viral-infected and uninfected cell population with flow cytometory (**Figure 3B**).

EPITOPE MAPPING OF MAbs

To determine the binding domain of the MAbs within the HPIV3-HN protein, we synthesized six different deletion mutants of HPIV3-HN as depicted in **Figure 4A**. All of the deletion mutants contained N-terminal biotin tag were incubated with the antibodies (#7, #21, or #23), followed by the addition of AlphaScreen streptavidin donor and protein A acceptor beads, as depicted in **Figure 4B**. The reactivity was measured and calculated by the level of the AlphaScreen luminescent signal. The results showed that two MAbs (#7 and #23) reacted against the cytoplasmic tail (CT) of HPIV3-HN whereas #21 MAb detected extracellular stalk region of the protein (**Figures 4C–E**). This result is fully consistent with the result of flow cytometry analysis (**Figure 3B**).

SPECIFICITY OF MAb

We next investigate the specificity of MAbs using HN protein frangments derived from HPIV1, Sendai virus (SeV), HPIV2, and Mumpus virus (MuV). Partial HN protein fragments containing cytoplasmic tail (CT), transmembrane domain (TM), and stalk region were produced with a N-terminal biotin tag by wheat cell-free system, and then incubated with the antibodies (#7, #21, or #23) followed by the AlphaScreen (**Figure 5A**). The antigen reactivity was measured based on the level of the AlphaScreen luminescent signal (**Figure 5B**). Notably, there was no cross-reactivity to HN proteins derived from other Paramyxoviruses except for HPIV3. This was also confirmed by immunoblotting analysis (**Figure 5C**). These results indicate the specificity of the antibodies for HPIV3-HN.

PROTEOMIC ANALYSIS

We next utilized our newly developed #21 MAb for the identification of host proteins that bind to HPIV3-HN during HPIV3 infection. Cell lysate from HPIV3-infected or mock-infected cells were immunoprecipitated with #21 MAb. Precipitated samples were collected and then digested with trypsin followed by LC-MS/MS analysis (**Figure 6A**). Annotation analysis using the Swiss-Prot database revealed that 10 proteins were putative HN binding proteins (**Figure 6B**). Based on the number of corrected peptides, top four proteins (HSP70, HSP90, tubulin, alpha 1c, and SERPINA3) were selected as the most likely candidates for association with HN and subjected to further binding analysis. The pull-down analysis of the host proteins with recombinant HPIV3-HN was performed. The subsequent immunoblotting analysis demonstrated that HPIV3-HN could indeed interact with these four proteins (**Figure 6C**). These results demonstrate the availability of our newly-developed antibody in comprehensive proteomic analysis.

DISCUSSION

Herein we produced HPIV3-HN proteins by the wheat cell-free system, and created MAbs that selectively target the HPIV3-HN protein. Characterization of the most potent MAb confirmed the antigen-specificity and usability in various applications including immunoblotting, immnofluorescent, flow cytometry, and immunoprecipitation analyses. Furthermore, the MAb could capture the endogenous HN protein from HPIV3-infected cells to identify HN-binding host proteins via mass spectrometry-based proteomic analysis. Our current results demonstrated the generation of useful antibody against HPIV3-HN and also shed new light

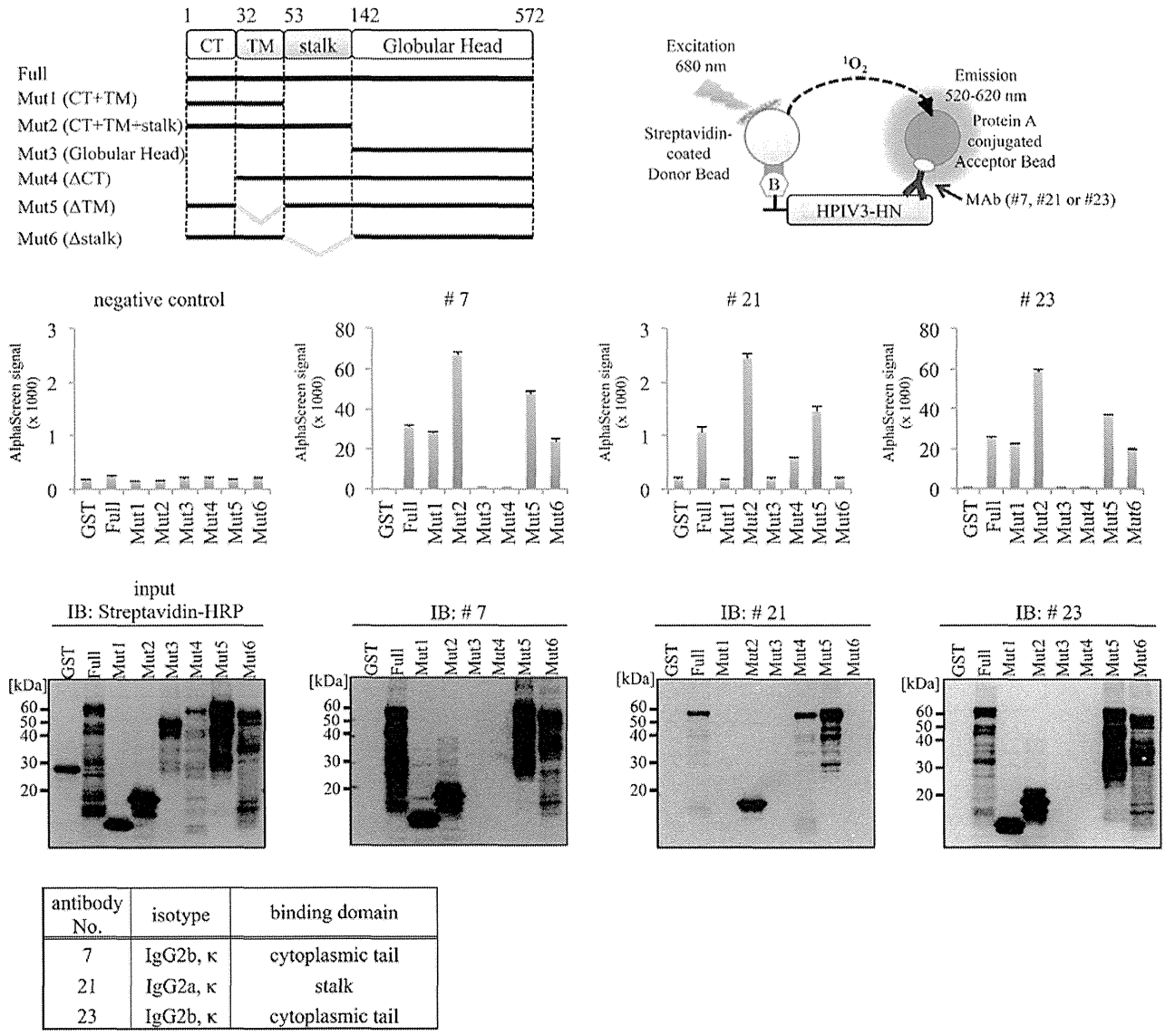

antibody No.	isotype	binding domain
7	IgG2b, κ	cytoplasmic tail
21	IgG2a, κ	stalk
23	IgG2b, κ	cytoplasmic tail

FIGURE 4 | Epitope mapping for generated antibodies. (A) Schematic diagram of seven deletion mutants of HPIV3-HN for epitope mapping. These proteins were produced as N-terminal biotinylated protein by wheat germ cell-free system. **(B)** Schematic diagram of the AlphaScreen assay used to detect the binding of MAb to full-length or deletion mutants of HPIV3-HN. The interaction between antibodies and recombinant proteins was monitored by AlphaScreen with protein A-conjugated acceptor beads and streptavidin-coated donor. Upon excitation at 680 nm, singlet oxygen molecules were produced from the donor beads, which reacted with the acceptor beads, resulting in light emission that was measured between 520 and 620 nm. **(C)** In AlphaScreen assay, the binding activity was measured as the level of the AlphaScreen luminescence signal. Error bars represent standard deviations from three independent experiments. **(D)** The biotinylated-full-length HN, its deletion mutants and GST proteins were separated by SDS-PAGE and transferred to PVDF membrane, followed by immunoblotting with Strepavidin-HRP andibody (left panel) and indicated MAb (right panel). **(E)** Summary of properties of selected MAbs. Immunoglobulin isotyping was carried out with mouse monoclonal antibody isotyping test kit.

on the unexplored molecular link between the PIV3-HN and host proteins.

Currently, cell-based production (e.g., *E. coli* system or baculovirus-insect cell system) of recombinant virus proteins has been widely used. However, it is often difficult to produce sufficient quantities of viral antigens in the conventional cell-based system because many viral antigens are usually insoluble, cytotoxic, and are expressed in the inclusion body fraction. In contrast, the cell-fee protein production system enables the synthesis of toxic proteins that are otherwise excluded from production in live cells. Among the cell-free approaches, the wheat germ cell-free system employs a eukaryotic translation system that warrants the synthesis of properly folded and biologically active proteins similar to proteins that are expressed in living mammalian cells (Endo and Sawasaki, 2005, 2006). These advantages underscore the suitability and availability of the wheat germ cell-free system for the generation of antigenic proteins that can be used for animal immunizations to generate

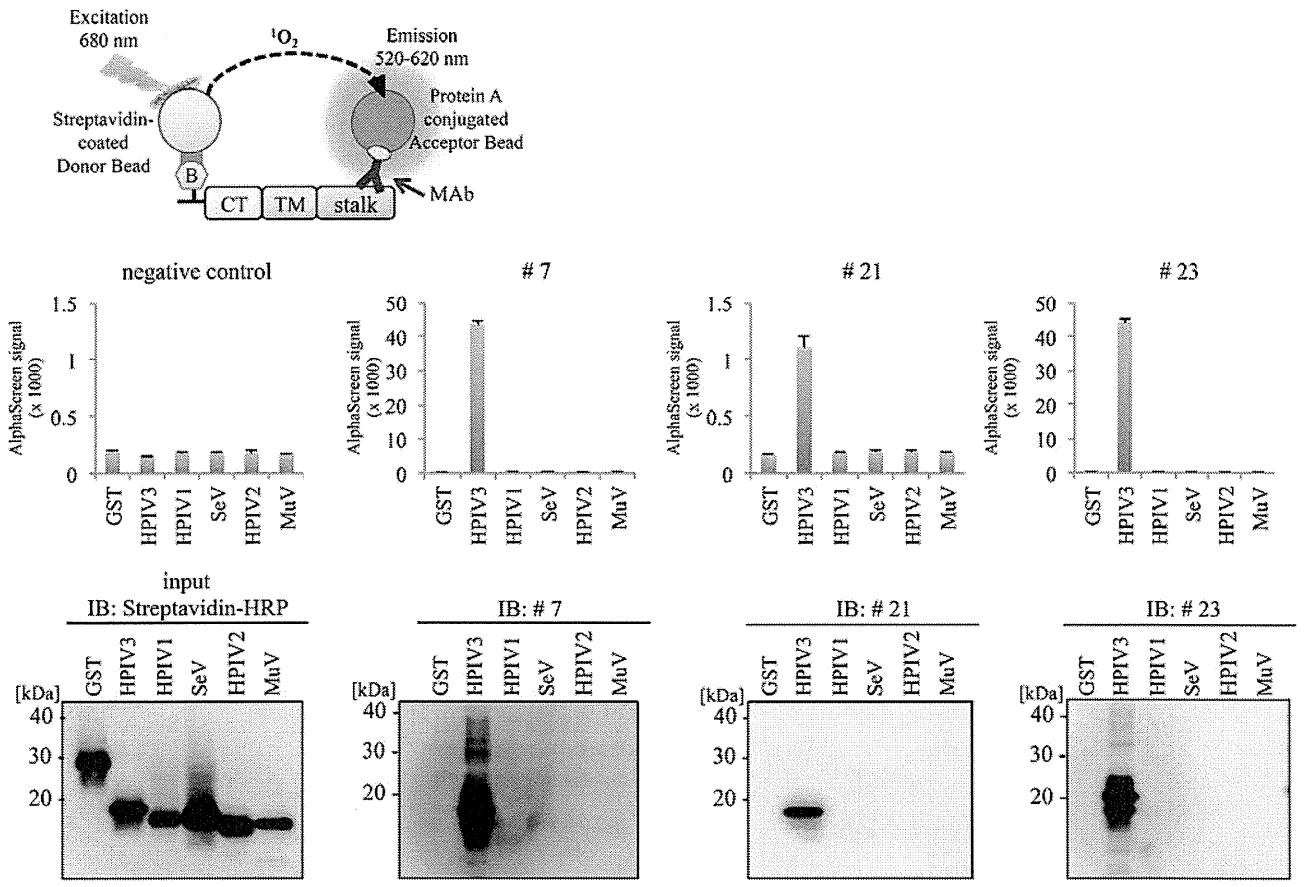

FIGURE 5 | No evident cross-reactivity of selected MAb to other paramyxoviruses. (A) Schematic diagram of AlphaScreen assay. The biotinylated partial HN proteins derived from several paramyxoviruses containing CT, TM and stalk region were produced by wheat germ cell-free system. **(B,C)** Specificity of MAbs was varidated by AlphaScreen assay **(B)** and immunoblotting **(C)**. In AlphaScreen assay, the binding activity was measured as the level of the AlphaScreen luminescence signal **(B)**. Error bars represent standard deviations from three independent experiments. The biotinylated partial HN proteins were separated by SDS-PAGE and transferred to PVDF membrane, followed by immunoblotting with either Strepavidin-HRP andibody (left panel) or anti-HN MAbs (right panel; **C**).

MAbs. Our current study clearly demonstrated the benefit of using viral proteins synthesized by the wheat germ cell-free system to efficiently produce the MAbs against the viral antigen. Using this approach, we have created MAbs against HPIV3-HN that detected both denatured and native forms of the antigen. These MAbs were useful in various immunological assays including ELISA, IF, immunoblotting, and immunoprecipitation. Further careful studies of structural aspects are needed to determine whether the MAb can affect the virus infectivity.

We identified Hsp70 as a putative HN binding protein. Several previous studies demonstrated that Hsp70 was involved in the regulation of other RNA viruses. Hsp70 is known to associate with viral PB1 and PB2 subunits of influenza A virus, and it negatively regulated the expression of viral proteins in infected cells (Li et al., 2011). In another study, Hantavirus infection induced the expression of HSP70 that interacted with nucleocapsid protein and its overexpression suppressed viral infection in Vero E6 cells (Yu et al., 2009). In contrast, Hsp70 was found to positively regulate rabies viral infection. Indeed, rabies infection induced the cellular expression of Hsp70 and accumulation in Negri body-like structures, which are the site of viral transcription and replication. Inhibition of Hsp70 resulted in a significant decrease of viral mRNAs, viral proteins, and virus particles (Lahaye et al., 2009, 2012). Taken together these results indicated a pivotal role of Hsp70 in viral replication and the pathogenicity of viral infection. Hsp70 binds and regulates many cellular proteins, as well as viral proteins (Pratt and Toft, 2003; Mayer, 2005; Silver and Noble, 2012), and the effects of Hsp70 on viral infection are diverse and unique between different viral species or cell systems. Further studies are required to investigate the precise molecular mechanism by which the association of Hsp70 and HN proteins mediate HPIV3 replication.

We also found that PIV3-HN can interact with Serpin3a. Serpin3a, as also known as alpha-1-antichymotrypsin, is a member of serpin proteins involved in the inhibition of serine and other types of proteases (Bauman et al., 2002). In humans, the majority

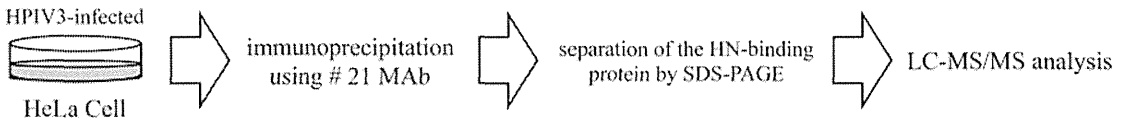

Accession number	name	peptide	Da	Molecular function	Subcellular localization
P08107	HSP70	10	70,052	Chaperone	cytoplasm
P08238	HSP90	6	83,264	Chaperone	cytoplasm
Q9BQE3	Tubulin alpha-1C	6	49,895	structural constituent of cytoskeleton	cytoplasm, cytoskeleton, microtubule
P01011	SERPINA3	6	47,651	protease inhibitor	secreted
P07195	LDH-B	5	36,638	oxidoreductase	cytoplasm
P04406	GAPDH	5	36,053	oxidoreductase, transferase	cytoplasm, cytoskeleton, membrane, nucleus
P10809	HSP60	4	61,055	chaperone	mitochondrion
P06733	MBP-1	4	47,169	lyase, repressor	cell membrane, cytoplasm, membrane, nucleus
P14618	PKM	4	57,937	kinase, transferase	cytoplsdm, nucleus
P60842	eIF4A1	3	46,154	helicase, hydrolase, initiation factor	cytoplasm

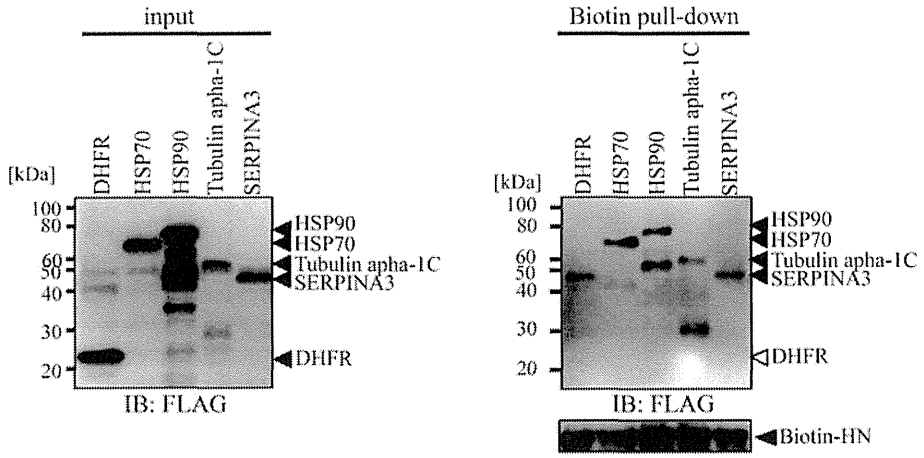

FIGURE 6 | Proteomics analysis using selected MAb. (A) Schematic diagram of proteomic analysis for the identification of PIV3-HN-binding protein. HPIV3-infected HeLa cell lysate was immunoprecipitated with #21 MAb. The bound proteins were separated by SDS-PAGE and analyzed by LC-Ms/Ms. **(B)** The panel shows the list of putative HN-binding proteins identified by mass spectrometry analysis. **(C)** FLAG-tagged HSP70, HSP90, tubulin alpha 1C, or SERPINA3 proteins were mixed with HPIV3-HN. Samples were pull-down with the streptavidin magnetic beads and the collected proteins were separated by SDS-PAGE. The bound protein detected by immunoblotting analysis with anti-FLAG antibody. The right arrows indicated the position of each protein.

of serpins regulates the functions of proteases involved in the response against body's injuries such as coagulation, fibrinolysis, inflammation, wound healing and tissue repair. Serpins have been also implicated in various pathologies in respiratory system such as airway hyperresponsiveness (AHR) and asthma (Sivaprasad et al., 2011). The physical interaction of HPIV3-HN with serpin3a may be involved in hindering the function of Serpin3a toward respiratory disorders. Further analysis may shed new light on understanding the etiology of HPIV3-induced asthma.

In summary, we utilized the wheat cell-free production system to create and characterize MAbs that may be useful in various immunological applications. Our newly-developed MAbs could thus provide a valuable means to explore HPIV3 infection in human cells.

ACKNOWLEDGMENTS

We thank Tomoe Suzuki for technical assistance, and Dr. Kei Miyakawa for FACS analysis. This work was partially supported by the fund for Creation of Innovation Centers for Advanced Interdisciplinary Research Areas Program in the Project for Developing Innovation Systems from the Ministry of Education, Culture, Sports, Science and Technology, and Research Grants from The Ministry of Health Labour and Welfare of Japan to Akihide Ryo.

REFERENCES

Ali, A., and Nayak, D. P. (2000). Assembly of Sendai virus: M protein interacts with F and HN proteins and with the cytoplasmic tail and transmembrane domain of F protein. *Virology* 276, 289–303. doi: 10.1006/viro.2000.0556

Bauman, S. J., Whinna, H. C., and Church, F. C. (2002). Serpins (serine protease inhibitors). *Curr. Protoc. Protein Sci.* Chap. 21, Unit 21.7. doi: 10.1002/0471140864.ps2107s26

Beck, E. T., He, J., Nelson, M. I., Bose, M. E., Fan, J., Kumar, S., et al. (2012). Genome sequencing and phylogenetic analysis of 39 human parainfluenza virus type 1 strains isolated from 1997–2010. *PLoS ONE* 7:e46048. doi: 10.1371/journal.pone.0046048

Chu, F. L., Wen, H. L., Hou, G. H., Lin, B., Zhang, W. Q., Song, Y. Y., et al. (2013). Role of N-linked glycosylation of the human parainfluenza virus type 3 hemagglutinin-neuraminidase protein. *Virus Res.* 174, 137–147. doi: 10.1016/j.virusres.2013.03.012

Counihan, M. E., Shay, D. K., Holman, R. C., Lowther, S. A., and Anderson, L. J. (2001). Human parainfluenza virus-associated hospitalizations among children less than five years of age in the United States. *Pediatr. Infect. Dis. J.* 20, 646–653. doi: 10.1097/00006454-200107000-00003

Endo, Y., and Sawasaki, T. (2005). Advances in genome-wide protein expression using the wheat germ cell-free system. *Methods Mol. Biol.* 310, 145–167. doi: 10.1007/978-1-59259-948-6_11

Endo, Y., and Sawasaki, T. (2006). Cell-free expression systems for eukaryotic protein production. *Curr. Opin. Biotechnol.* 17, 373–380. doi: 10.1016/j.copbio.2006.06.009

Glezen, W. P., Frank, A. L., Taber, L. H., and Kasel, J. A. (1984). Parainfluenza virus type 3: seasonality and risk of infection and reinfection in young children. *J. Infect. Dis.* 150, 851–857. doi: 10.1093/infdis/150.6.851

Goswami, K. K., and Russell, W. C. (1983). Monoclonal antibodies against human paramyxovirus type 3 and against SV5 virus: preparation and preliminary characterization. *J. Gen. Virol.* 64, 1663–1672. doi: 10.1099/0022-1317-64-8-1663

Horvath, C. M., Paterson, R. G., Shaughnessy, M. A., Wood, R., and Lamb, R. A. (1992). Biological activity of paramyxovirus fusion proteins: factors influencing formation of syncytia. *J. Virol.* 66, 4564–4569.

Hu, X. L., Ray, R., and Compans, R. W. (1992). Functional interactions between the fusion protein and hemagglutinin-neuraminidase of human parainfluenza viruses. *J. Virol.* 66, 1528–1534.

Huberman, K., Peluso, R. W., and Moscona, A. (1995). Hemagglutinin-neuraminidase of human parainfluenza 3: role of the neuraminidase in the viral life cycle. *Virology* 214, 294–300. doi: 10.1006/viro.1995.9925

Kimura, K., Nozaki, N., Enomoto, T., Tanaka, M., and Kikuchi, A. (1996). Analysis of M phase-specific phosphorylation of DNA topoisomerase II. *J. Biol. Chem.* 271, 21439–21445. doi: 10.1074/jbc.271.35.21439

Kimura, K., Nozaki, N., Saijo, M., Kikuchi, A., Ui, M., and Enomoto, T. (1994). Identification of the nature of modification that causes the shift of DNA topoisomerase II beta to apparent higher molecular weight forms in the M phase. *J. Biol. Chem.* 269, 24523–24526.

Lahaye, X., Vidy, A., Fouquet, B., and Blondel, D. (2012). Hsp70 protein positively regulates rabies virus infection. *J. Virol.* 86, 4743–4751. doi: 10.1128/JVI.06501-11

Lahaye, X., Vidy, A., Pomier, C., Obiang, L., Harper, F., Gaudin, Y., et al. (2009). Functional characterization of Negri bodies (NBs) in rabies virus-infected cells: evidence that NBs are sites of viral transcription and replication. *J. Virol.* 83, 7948–7958. doi: 10.1128/JVI.00554-09

Li, G., Zhang, J., Tong, X., Liu, W., and Ye, X. (2011). Heat shock protein 70 inhibits the activity of Influenza A virus ribonucleoprotein and blocks the replication of virus *in vitro* and *in vivo*. *PLoS ONE* 6:e16546. doi: 10.1371/journal.pone.0016546

Mayer, M. P. (2005). Recruitment of Hsp70 chaperones: a crucial part of viral survival strategies. *Rev. Physiol. Biochem. Pharmacol.* 153, 1–46. doi: 10.1007/s10254-004-0025-5

Miura, N., Nakatani, Y., Ishiura, M., Uchida, T., and Okada, Y. (1985). Molecular cloning of a full-length cDNA encoding the hemagglutinin-neuraminidase glycoprotein of Sendai virus. *FEBS Lett.* 188, 112–116. doi: 10.1016/0014-5793(85)80885-1

Momoki, T. S. (2013). Genotyping of mumps virus detected in Yokohama City from 1999 to 2010. *Jpn. J. Infect. Dis.* 66, 226–231. doi: 10.7883/yoken.66.226

Porotto, M., Greengard, O., Poltoratskaia, N., Horga, M. A., and Moscona, A. (2001). Human parainfluenza virus type 3 HN-receptor interaction: effect of 4-guanidino-Neu5Ac2en on a neuraminidase-deficient variant. *J. Virol.* 75, 7481–7488. doi: 10.1128/JVI.75.16.7481-7488.2001

Porotto, M., Palmer, S. G., Palermo, L. M., and Moscona, A. (2012). Mechanism of fusion triggering by human parainfluenza virus type III: communication between viral glycoproteins during entry. *J. Biol. Chem.* 287, 778–793. doi: 10.1074/jbc.M111.298059

Pratt, W. B., and Toft, D. O. (2003). Regulation of signaling protein function and trafficking by the hsp90/hsp70-based chaperone machinery. *Exp. Biol. Med. (Maywood)* 228, 111–133.

Rydbeck, R., Orvell, C., Love, A., and Norrby, E. (1986). Characterization of four parainfluenza virus type 3 proteins by use of monoclonal antibodies. *J. Gen. Virol.* 67, 1531–1542. doi: 10.1099/0022-1317-67-8-1531

Sawasaki, T., Kamura, N., Matsunaga, S., Saeki, M., Tsuchimochi, M., Morishita, R., et al. (2008). Arabidopsis HY5 protein functions as a DNA-binding tag for purification and functional immobilization of proteins on agarose/DNA microplate. *FEBS Lett.* 582, 221–228. doi: 10.1016/j.febslet.2007.12.004

Silver, J. T., and Noble, E. G. (2012). Regulation of survival gene hsp70. *Cell Stress Chaperones* 17, 1–9. doi: 10.1007/s12192-011-0290-6

Sivaprasad, U., Askew, D. J., Ericksen, M. B., Gibson, A. M., Stier, M. T., Brandt, E. B., et al. (2011). A nonredundant role for mouse Serpinb3a in the induction of mucus production in asthma. *J. Allergy Clin. Immunol.* 127, 254–261. doi: 10.1016/j.jaci.2010.10.009

Skiadopoulos, M. H., Vogel, L., Riggs, J. M., Surman, S. R., Collins, P. L., and Murphy, B. R. (2003). The genome length of human parainfluenza virus type 2 follows the rule of six, and recombinant viruses recovered from non-polyhexameric-length antigenomic cDNAs contain a biased distribution of correcting mutations. *J. Virol.* 77, 270–279. doi: 10.1128/JVI.77.1.270-279.2003

Stone, R., and Takimoto, T. (2013). Critical role of the fusion protein cytoplasmic tail sequence in parainfluenza virus assembly. *PLoS ONE* 8:e61281. doi: 10.1371/journal.pone.0061281

Storey, D. G., Dimock, K., and Kang, C. Y. (1984). Structural characterization of virion proteins and genomic RNA of human parainfluenza virus 3. *J. Virol.* 52, 761–766.

Takahashi, H., Takahashi, C., Moreland, N. J., Chang, Y. T., Sawasaki, T., Ryo, A., et al. (2012). Establishment of a robust dengue virus NS3-NS5 binding assay for identification of protein-protein interaction inhibitors. *Antiviral Res.* 96, 305–314. doi: 10.1016/j.antiviral.2012.09.023

Takai, K., and Endo, Y. (2010). The cell-free protein synthesis system from wheat germ. *Methods Mol. Biol.* 607, 23–30. doi: 10.1007/978-1-60327-331-2_3

Takai, K., Sawasaki, T., and Endo, Y. (2010). The wheat-germ cell-free expression system. *Curr. Pharm. Biotechnol.* 11, 272–278. doi: 10.2174/138920110791111933

Takimoto, T., Taylor, G. L., Connaris, H. C., Crennell, S. J., and Portner, A. (2002). Role of the hemagglutinin-neuraminidase protein in the mechanism of paramyxovirus-cell membrane fusion. *J. Virol.* 76, 13028–13033. doi: 10.1128/JVI.76.24.13028-13033.2002

Tashiro, M., and Homma, M. (1985). Protection of mice from wild-type Sendai virus infection by a trypsin-resistant mutant, TR-2. *J. Virol.* 53, 228–234.

van Wyke Coelingh, K. L., Winter, C., and Murphy, B. R. (1985). Antigenic variation in the hemagglutinin-neuraminidase protein of human parainfluenza type 3 virus. *Virology* 143, 569–582. doi: 10.1016/0042-6822(85)90395-2

Waner, J. L., Whitehurst, N. J., Downs, T., and Graves, D. G. (1985). Production of monoclonal antibodies against parainfluenza 3 virus and their use in diagnosis by immunofluorescence. *J. Clin. Microbiol.* 22, 535–538.

Wechsler, S. L., Lambert, D. M., Galinski, M. S., Heineke, B. E., and Pons, M. W. (1985). Human parainfluenza virus 3: purification and characterization of subviral components, viral proteins and viral RNA. *Virus Res.* 3, 339–351. doi: 10.1016/0168-1702(85)90434-4

Weinberg, G. A., Hall, C. B., Iwane, M. K., Poehling, K. A., Edwards, K. M., Griffin, M. R., et al. (2009). Parainfluenza virus infection of young children: estimates of the population-based burden of hospitalization. *J. Pediatr.* 154, 694–699. doi: 10.1016/j.jpeds.2008.11.034

Yu, L., Ye, L., Zhao, R., Liu, Y.F., and Yang, S.J. (2009). HSP70 induced by Hantavirus infection interacts with viral nucleocapsid protein and its overexpression suppresses virus infection in Vero E6 cells. *Am. J. Transl. Res.* 1, 367–380.

Conflict of Interest Statement: The authors declare that the research was conducted in the absence of any commercial or financial relationships that could be construed as a potential conflict of interest.

Received: 24 February 2014; accepted: 18 April 2014; published online: 13 May 2014.
Citation: Matsunaga S, Kawakami S, Matsuo I, Okayama A, Tsukagoshi H, kudoh A, Matsushima Y, Shimizu H, Okabe N, Hirano H, Yamamoto N, Kimura H and Ryo A (2014) Wheat germ cell-free system-based production of hemagglutinin-neuraminidase glycoprotein of human parainfluenza virus type 3 for generation and characterization of monoclonal antibody. Front. Microbiol. 5:208. doi: 10.3389/fmicb.2014.00208

This article was submitted to Virology, a section of the journal Frontiers in Microbiology.

JOURNAL OF PROTEOMICS 115 (2015) 132–142

Available online at www.sciencedirect.com

ScienceDirect

www.elsevier.com/locate/jprot

Augmentation of multiple protein kinase activities associated with secondary imatinib resistance in gastrointestinal stromal tumors as revealed by quantitative phosphoproteome analysis

Kayoko Nagata[a], *Takao Kawakami*[a,b], *Yoichi Kurata*[a], *Yayoi Kimura*[a], *Yusuke Suzuki*[a], *Takashi Nagata*[c], *Yuji Sakuma*[d], *Yohei Miyagi*[d], *Hisashi Hirano*[a,*]

[a]*Advanced Medical Research Center/Graduate School of Medical Life Science, Yokohama City University, 3-9 Fukuura, Kanazawa, Yokohama 236-0004, Japan*

[b]*Biomolecule Analysis Group, Medical ProteoScope Company, 3-9 Fukuura, Kanazawa, Yokohama 236-0004, Japan*

[c]*Institute of Advanced Energy/Graduate School of Energy Science, Kyoto University, Gokasho, Uji Kyoto 611-0011, Japan*

[d]*Molecular Pathology and Genetics Division, Kanagawa Cancer Center Research Institute, 1-1-2 Nakao, Asahi, Yokohama 252-0373, Japan*

ARTICLE INFO

Article history:
Received 28 August 2014
Accepted 16 December 2014
Available online 29 December 2014

Keywords:
GIST
Imatinib
Phosphoproteomics
Acquired resistance
Targeted therapy

ABSTRACT

Mutations in the Kit receptor tyrosine kinase gene (*KIT*), which result in constitutive activation of the protein (KIT), are causally related to the development of gastrointestinal stromal tumors (GISTs). Imatinib, a targeted anticancer drug, exerts a therapeutic effect against GISTs by repressing the kinase activity of KIT. Long-term administration of this drug, however, causes the emergence of imatinib-resistant GISTs. We performed quantitative phosphoproteome analysis using a cell-based GIST model system comprising an imatinib-sensitive GIST cell line (GIST882), GIST882 under treatment with imatinib (GIST882-IM), and secondary imatinib-resistant GIST882 (GIST882-R). Phosphorylated peptides were purified from each cell line using titania-based affinity chromatography or anti-phosphotyrosine immunoprecipitation, and then subjected to LC-MS/MS based quantitative phosphoproteome analysis. Using this method we identified augmentation of the kinase activities of multiple elements of the signal transduction pathway, especially KIT and EGFR. Although, these elements were up-regulated in GIST882-R, no additionally mutated *KIT* mRNA was found in secondary imatinib-resistant GIST cells. Treatment of GIST882-R with imatinib in combination with gefitinib, an EGFR inhibitor, partially prevented cell growth, implying that EGFR may be involved in acquisition of secondary imatinib resistance in GIST.

Biological significance

In this study, we performed a quantitative phosphoproteome analysis using a cell culture-based GIST model system. The goal of the study was to investigate the mechanism

Abbreviations: GIST, gastrointestinal stromal tumor; KIT, mast/stem cell growth factor receptor Kit; PDGFRA, platelet-derived growth factor receptor alpha; RTK, receptor tyrosine kinase; EGFR, epidermal growth factor receptor; PI3K, phosphatidylinositol 3-kinase; Akt, protein kinase B; mTOR, mammalian target of rapamycin; MAPK, mitogen-activated protein kinase; ERK, extracellular signal-regulated kinases.

* *Corresponding author at:* 3-9 Fukuura, Kanazawa, Yokohama 236-0004, Japan. Tel.: +81 45 787 2993; fax: +81 45 787 2787.
E-mail address: hirano@yokohama-cu.ac.jp (H. Hirano).

http://dx.doi.org/10.1016/j.jprot.2014.12.012
1874-3919/

of acquired resistance in GISTs against imatinib, a molecularly targeted drug that inhibits kinase activity of the KIT protein and that has been approved for the treatment of GISTs. In imatinib-resistant GIST cells, we observed elevated expression of KIT and restoration of its kinase activity, as well as activation of multiple proliferative signaling pathways. Our results indicate that the effects of even so-called 'molecularly targeted' drugs, are broad rather than convergent, and that the mechanisms of action of such drugs during continuous administration are extremely complex.

1. Introduction

Gastrointestinal stromal tumors (GISTs) are the most common mesenchymal tumors of the digestive tract. GISTs may originate from the interstitial cells of Cajal (ICCs), which are mesenchymal pacemaker cells, and share ultrastructural and immunohistochemical features with ICCs [1–3]. The vast majority (85%) of GISTs have mutations in the gene encoding the Kit receptor tyrosine kinase (*KIT*), and 5–10% have mutations in the gene encoding platelet-derived growth factor receptor alpha (*PDGFRA*) [4–6]. KIT and PDGFRA are structurally homologous and belong to the type III receptor tyrosine kinase (RTK) family. KIT is activated upon binding to its ligand, stem cell factor (SCF), which leads to activation of signaling pathways including the PI3K/Akt/mTOR and Ras/Raf/MAPK cascades [7,8]. Thus, KIT prevents apoptosis and controls proliferation, adhesion, and differentiation [9]. These functions of KIT play important roles in the differentiation and proliferation of ICCs. Mutations of *KIT* found in GISTs result in constitutive activation of tyrosine kinase activity and downstream signaling pathways [1].

GISTs are generally resistant to conventional chemotherapy and radiation therapy; consequently, unresectable and/or metastatic cases are difficult to treat [10]. Based on recent findings regarding the biological relevance of KIT in GISTs, a selective tyrosine kinase inhibitor of BCR-ABL, KIT, and PDGFRA, imatinib mesylate (imatinib, STI571, or Gleevec; Novartis Pharma, Basel, Switzerland), has been administered to patients with advanced GISTs with the goal of determining its therapeutic effectiveness [11,12]. More than 40% of advanced GIST patients who received imatinib exhibited an objective response; among them, 85–90% exhibited improved control of disease [13]. Despite these encouraging early therapeutic results, resistance developed with a median time of 2 years after initiation of imatinib therapy; therefore, additional therapeutic strategies are desired [14]. GISTs may acquire secondary imatinib resistance by developing additional mutations in *KIT*, by activation of signal transduction pathways mediated by other kinases, and/or by activation of multidrug resistance genes [7,15].

In this study, we used a cell-based model system to investigate the molecular basis of the acquisition of secondary imatinib resistance in GIST. To this end, we generated a GIST cell line with secondary (acquired) imatinib resistance, GIST882-R, from the imatinib-sensitive line GIST882. To elucidate the cause of resistance, we performed MS-based quantitative phosphoproteome analysis, a robust method for the comprehensive elucidation of phosphorylation/dephosphorylation states of proteins that play key roles in the signal transduction cascades, especially in the context of biomedical science [16,17].

The cell-based model system that we developed for this study comprises GIST882 cell lines in three different states: GIST882, representing pretreatment; GIST882-IM, representing a tumor undergoing treatment; and GIST882-R, representing a tumor with acquired imatinib resistance. From each of these cell lines, we isolated phosphorylated peptides (phosphopeptides) and concentrated them by means of two distinct methods: titania-based affinity enrichment, which utilizes a titanium dioxide column, and immunoprecipitation (IP) enrichment, which utilizes an anti-phosphotyrosine antibody. The isolated phosphopeptides were then analyzed by LC-MS/MS.

Subsequently, we performed quantitative phosphoproteome analysis by direct comparison of phosphopeptide MS scan profiles. The results revealed that proteins involved in different signal transduction pathways exhibited distinct phosphorylation patterns, suggesting that the deviation of signal transduction pathways in GIST882-R from those in GIST882 caused the acquisition of its secondary imatinib resistance. Furthermore, we observed that the phosphorylation of epidermal growth factor receptor (EGFR) was upregulated in GIST882-R, suggesting that EGFR activation promotes proliferation in this cell line. Accordingly, we treated GIST882-R with an inhibitor for EGFR, gefitinib, together with imatinib, and found that this combination therapy partially suppressed cell growth.

2. Materials and methods

2.1. Generation of imatinib-resistant GIST cells

The GIST882 cell line was generous gift from Dr. Jonathan A. Fletcher (Department of Pathology, Brigham and Women's Hospital, Boston, MA, USA). To generate an imatinib-resistant cell line (GIST882-R), GIST882 cells were exposed to increasing concentrations of imatinib. Imatinib concentrations were increased stepwise from 10 nM to 200 nM. The concentration was changed to the next higher value when the cells resumed growth kinetics similar to that of the untreated parental cells. Cell viability assays were performed to confirm the emergence of the imatinib-resistant cells (section 2.2.). The resultant GIST882-R cells were maintained in 200 nM imatinib. All cells were cultured in RPMI GlutaMAX medium (Gibco BRL/Life Technologies, San Diego, CA, USA) supplemented with 20% fetal bovine serum (Gibco BRL/Life Technologies) and 0.2% Fungizone (Gibco BRL/Life Technologies), in a humidified 5% incubator at 37 °C in an atmosphere containing 5% CO_2.

2.2. Cell-viability assay

GIST882 and GIST882-R cells were seeded in 96-well plates at an appropriate density to reach ~80% confluence at the end of the assay. After 2 days of incubation at 37 °C, the cells were

exposed to imatinib at 16, 31, 63, 125, 250, 500, or 1000 nM for 3 days. Subsequently, 20 μL of CellTiter 96 AQueous One Solution reagent (Promega Co., Madison, WI, USA) was added to each well and incubated for an additional 2 h. Cell viability was measured by reading absorbance of each well at 492 nm on a plate reader (Infinite 200; Tecan Group Ltd., Männedorf, Switzerland). These assays were performed in triplicate and repeated independently three times. Data were expressed as the percentage survival relative to the control, calculated from the background-corrected absorbance values.

2.3. *KIT* sequence analysis

Total RNA was isolated from the GIST cell lines using a Nucleospin RNA column (Takara Bio, Otsu, Japan), and cDNA was synthesized using the PrimeScript First-Strand cDNA Synthesis Kit (Takara Bio) with an oligo-dT primer and random 6mers. For the *KIT* coding sequence analysis, sequencing templates were prepared in three different methods: i) The *KIT* cDNA was amplified by polymerase chain reaction (PCR) using KOD plus DNA polymerase (Toyobo, Osaka, Japan) and *KIT*-specific primers (sense 5′-GATCCCA TCGCAGCTACC-3′ and antisense 5′-CCCACTATCCTGGAGTT GGA-3′, corresponding respectively to nucleotides 67–84 and 3124–3105 of the *KIT* mRNA [GenBank accession number: NM_000222]). The PCR products were purified using the Wizard SV Gel and PCR Clean-up System (Promega); ii) The limiting-diluted *KIT* cDNA was amplified according to the previous report[18]; iii) The amplified *KIT* cDNA obtained in i) was cloned into pDM20 vector (TaKaRa Bio). DNA sequencing reactions were performed using the BigDye Terminator v3.1 Cycle Sequencing kit (Thermo Fisher Scientific, Waltham, MA, USA), and sequencing samples were analyzed on an ABI 3100 DNA sequencer (Applied Biosystems, Foster City, CA, USA). Sequence alignments and mutation scanning were performed using NCBI-BLAST (bl2seq). Sequencing analysis of the *KIT* cDNA obtained from GIST882 or GIST882-R cells by method (i) was performed five times and that of the *KIT* cDNA obtained from GIST882-R cells by method (ii) or (iii) was performed three times.

2.4. Preparation of peptide mixtures

Cells at about 80% confluence were washed twice with ice-cold PBS. After washing, cells were scraped into lysis buffer (20 mM HEPES-NaOH, pH 8.0, 9 M urea, 25 mM sodium pyrophosphate, 10 mM β-glycerophosphate, and 1% *v/v* each of Phosphatase Inhibitor Cocktail solutions 1 and 2 [Sigma-Aldrich, St. Louis, MO, USA]), followed by two rounds of sonication at 4 °C for 30 s each using a microtip sonication probe (Ultrasonic Disruptor UR-21P; Tomy Seiko, Tokyo, Japan). Sonicated cell lysates were clarified by centrifugation at 15,000 ×*g* for 10 min, and protein concentrations were determined using the Protein Assay CBB Solution (Nacalai Tesque, Kyoto, Japan). Aliquots were subjected to a cycle of dithiothreitol (DTT) reduction (4.1 mM, 60 °C, 20 min) and S-carboxyamidomethylation (8.3 mM iodoacetamide, room temperature, 15 min). The protein solutions were diluted 4-fold with 20 mM HEPES-NaOH, and then subjected to protein hydrolysis with bovine trypsin (tosyl phenylalanyl chloromethyl ketone (TPCK)-treated, Sigma-Aldrich) at room temperature for 16 h at an enzyme-to-substrate ratio of 1:20 (*w/w*). To stop hydrolysis, trifluoroacetic acid (TFA) was added to protein hydrolysates to a final concentration of 1%, and precipitates were removed by centrifugation at 2000 ×*g* for 5 min. The acidified hydrolysates were loaded onto StageTips [19] with SDB-XD Empore disks (3 M, St. Paul, MN, USA) or Oasis-HLB cartridges (1 mL barrel size, 30 mg sorbent; Waters, Milford, MA, USA) equilibrated with 0.1% TFA. Cartridges were washed with 0.1% TFA, followed by a serial elution of peptides with 10, 20, 30, 40, and 50% acetonitrile in 0.1% TFA. All peptide fractions were pooled and lyophilized.

2.5. Enrichment of phosphopeptides using titania-based affinity chromatography

TiO_2 tip columns were prepared using C8 StageTips with C8 Empore disks (3 M) and TiO_2 bulk beads (3 mg of 10 μm Titansphere TiO_2 beads per 200 μL pipette tip; GL Sciences, Tokyo, Japan) [20]. One hundred micrograms of peptide mixture (Section 2.4) was loaded onto the TiO_2 tip column according to the manufacturer's instructions for the Titansphere Phos-Tio Kit (GL Science). Peptides were eluted with 50 μL each of 5% ammonium hydroxide and 5% pyrrolidine. Eluted peptide fractions were collected together and immediately acidified with TFA to pH < 3. The peptide solution was desalted using the SDB-XD StageTips, and then concentrated in a vacuum evaporator. One-quarter of the lyophilized peptide sample was subjected to LC-MS/MS.

2.6. Enrichment of phosphopeptides using an anti-phosphotyrosine antibody

A peptide mixture derived from 3 mg protein (Section 2.4.) was dissolved in 400 μL of immunoprecipitation (IP) buffer (50 mM 3-morpholinopropane-1-sulfonic acid [MOPS]-NaOH [pH 7.2], 10 mM sodium phosphate, 50 mM NaCl), and insoluble matter was removed by centrifugation at 2000 ×*g* for 5 min. Phospho-tyrosine mAb (P-Tyr-100) beads (Cell Signaling Technology, Danvers, MA, USA) was used to pull down pY peptides from the peptide mixtures [21]. Ten microliters of antibody bead slurry (50%) was added to the peptide mixtures, and the suspensions were incubated overnight at 4 °C with gentle rotation. The antibody beads were washed three times with 500 μL IP buffer and once with 500 μL water. All of the washing steps were performed at 4 °C. Peptides were eluted from beads by incubation with 100 μL of 0.15% TFA at room temperature for 10 min. Non-specifically bound proteins in the eluted fractions were then removed using TiO_2 tip columns (Section 2.5.). Finally, the purified peptide fractions were desalted with the SDB-XD StageTips and concentrated in a vacuum evaporator.

2.7. LC-MS/MS analysis

Phosphopeptide samples were analyzed using an LTQ-Orbitrap Velos hybrid mass spectrometer (Thermo Fisher Scientific) in a fully automated manner. Briefly, peptide separation was performed with an UltiMate 3000 LC system (Dionex, LC Packings, Sunnyvale, CA, USA) containing a C18 capillary LC column (Acclaim PepMap100 C18 column, 75 μm i.d., 150 mm length, 3 μm particle size, and 100 Å pore size; Thermo Fisher Scientific). The mobile phase consisted of formic acid, acetonitrile, and water at a volume ratio of 0.1:2:98 for mobile phase A,

and 0.1:95:5 for mobile phase B. The peptides were continuously eluted at a rate of 300 nL/min in gradient mode: the initial proportion of 2% mobile phase B was increased linearly to 33% B during 115 min, and subsequently increased to 95% B during the next 10 min. Protonated peptides in the gas phase were analyzed sequentially by MS/MS in Data-Dependent Scanning mode, consisting of a full-range scan in the *m/z* range of 350 to 1200 and subsequent product ion scans for each of the fifteen most intense ions in the full-scan mass spectrum.

2.8. *Label-free quantitation and peptide identification*

Label-free relative peptide quantitation was performed by direct comparison of each MS scan profile using the Progenesis LC-MS data analysis software (version 4.1, Nonlinear Dynamics, Durham, NC, USA). The obtained normalized abundances of each peptide were subjected to statistical analysis using one-way analysis of variance (ANOVA). In this study, the detected feature was assumed to be statistically significant when the *p*-value for a given peptide was <0.05. To identify the sequence of peptides, peak lists were created using Progenesis LC-MS. The obtained MS and MS/MS data were searched against human protein sequences (20,233 entries) in the Swiss-Prot database (January, 2013) using the MASCOT software, version 2.4.1 (Matrix Science, London, UK). The search parameters were as follows: trypsin digestion with two missed cleavages permitted; variable modifications: N-terminal carbamylation, protein N-terminal acetylation, S-carbamidomethylation of cysteine, oxidation of methionine, and phosphorylation of serine, threonine and tyrosine; peptide tolerance of ±5 ppm; and an MS/MS tolerance of ± 0.5 Da. FDR (false discovery rate) estimation was performed on a decoy database using the MASCOT software. We used 1% FDR as a cut-off for exporting results from the analysis.

2.9. *Gene ontology enrichment analysis*

To elucidate the biological functions of the identified proteins, Gene Ontology (GO) enrichment analysis was performed using the Database for Annotation, Visualization, and Integrated Discovery (DAVID) v6.7 (http://david.abcc.ncifcrf.gov/) [22,23]. All identified proteins in this study were used as background, and the level of significance was set to $p < 0.01$.

2.10. *Western blotting*

Cell lysates were prepared using lysis buffer (20 mM HEPES-NaOH, pH 8.0, 9 M urea, 1% *v/v* each of Phosphatase Inhibitor Cocktail solutions 1 and 2 [Sigma-Aldrich], and Complete Protease Inhibitor mixture [Roche Diagnostics]). Extracts were subjected to SDS PAGE, and the resolved proteins were transferred onto PVDF membranes. After blocking non-specific binding with Blocking One solution (Nacalai Tesque), the PVDF membranes were incubated with primary antibodies at 4 °C overnight. Primary antibodies were as follows: anti-KIT (sc-168; Santa Cruz Biotechnology, Dallas, TX, USA); anti-phospho-KIT Y703 (44-492; BD Biosciences, San Diego, CA, USA); anti-actin (sc-1616, Santa Cruz Biotechnology); anti-ERK 1/2 (9102, Cell Signaling Technology); anti-phospho-ERK 1/2 Thr202/Tyr204 (9101, Cell Signaling Technology); anti-c-JUN (9165, Cell Signaling Technology); anti-phospho-c-JUN Ser63 (2361, Cell Signaling Technology); anti-PDGFRα (3174, Cell Signaling Technology); and anti-EGFR (sc-03, Santa Cruz Biotechnology). The membranes were then washed three times with TBS-T (20 mM Tris–HCl, pH 7.5, 150 mM NaCl, and 0.05% Tween-20). Next, the membranes were incubated with horseradish peroxidase (HRP)-conjugated secondary antibodies at room temperature for 1.5 h, followed by five washes with TBS-T. Immunoreactive protein bands were visualized using Chemi-Lumi One Super (Nacalai Tesque). To detect the protein bands, the membranes were scanned on a LAS-4000mini imaging system (GE Healthcare, Little Chalfont, UK). Western blotting analyses were performed at least twice, and band intensities were quantified using MultiGauge 3.0 software (Fujifilm, Tokyo, Japan).

2.11. *Quantitative real-time PCR*

Real-time PCR to detect the *KIT* and *EGFR* mRNAs was performed on an Mx3000P Real-Time QPCR System (Agilent Technologies, Santa Clara, CA, USA) using SYBR Premix Ex Taq II Perfect Real Time (Takara Bio). The primer pairs were as follows: *KIT*, 5′-ACTTAGAAGACTTGCTGAGC-3′ (forward) and 5′-TTGATGTCTGGCTAGACC-3′ (reverse); *EGFR*, 5′-CGTTCGGC ACGGTGTATAAG-3′ (forward) and 5′-GTTGGCTTTCGGAGA TGTTG-3′ (reverse); and *GAPDH*, 5′-GGTATCGTGGAAGGACT CATGAC-3′ (forward) and 5′-ATGCCAGTGAGCTTCCCGTT CAG-3′ (reverse). Each primer pair was used at a concentration of 400 nM. The relative expression levels of *KIT* and *EGFR* mRNA were normalized to that of *GAPDH* mRNA using the ΔΔCt method.

2.12. *Combined administration of imatinib and gefitinib*

GIST882 cells and GIST882-R cells were seeded separately in 96-well plates. After a 2-day incubation, the cells were exposed to imatinib at 100 nM, 200 nM, or 500 nM for 3 days. To each concentration of imatinib, gefitinib (Tocris Bioscience, Avonmouth, UK) was added at 250 nM, 500 nM, or 1000 nM. The cell viability was then measured as described in Section 2.2.

3. Results and discussion

3.1. *Development and characterization of GIST882-R, a secondary imatinib-resistant GIST882 cell line*

GIST882 is a GIST cell line that has an activating homozygous missense mutation in *KIT* exon 13, encoding a KIT oncoprotein harboring the K642E mutation [24]. GIST882 cells were exposed to increasing concentrations of imatinib, resulting in the acquisition of imatinib resistance. We named this secondary (acquired) imatinib-resistant GIST882 cell line GIST882-R. To ascertain imatinib sensitivity, cell viability assays were performed by calculating the half-maximal inhibitory concentration (IC_{50}). The imatinib IC_{50} value of GIST882-R (ca. 270 nM) was more than 3-fold higher than that of GIST882 (ca. 80 nM) (Fig. 1A). Growth of GIST882 was effectively inhibited by imatinib at low

concentrations (ca. <100 nM); however, higher concentrations of imatinib did not further decrease the cell viability of GIST882, which stayed constant at ~30% (ca. >100 nM). By contrast, cell viability of GIST882-R was effectively inhibited (cell viability of ~20%) by administration of imatinib at high concentrations (ca. >500 nM). Notably, imatinib treatment decreased the cell viability of GIST882-R below that of GIST882.

Next, the expression and phosphorylation levels of KIT were analyzed by western blotting. KIT is generally observed as two bands [25], corresponding to fully glycosylated membrane-bound KIT and immature KIT protein [26–28]; our observations were consistent with these reports (Fig. 1B). The intensities of the bands indicated that expression of KIT, especially the fully glycosylated form, was higher in GIST882-R than in GIST882.

Autophosphorylation of KIT at residue Y703 is important for the activation of downstream signal transduction pathways [29]. We grew GIST882-R and GIST882 in media containing 200 and 0 nM imatinib, respectively, and inspected the amount of the phosphorylated Y703 in each cell line. Phosphorylation levels of KIT at Y703 were slightly elevated in GIST882-R relative to GIST882 (Fig. 1B).

GIST is believed to acquire secondary imatinib resistance by developing additional mutations in *KIT* (i.e., beyond the original mutations), by activation of signal transduction pathways mediated by other kinases, and/or by activation of multidrug resistance genes [7,15]. Usually the resistance mechanism is due to the secondary mutation in *KIT* [30]. However, there are no *KIT* additional mutations in GIST882-R mRNA. This was confirmed by sequencing of three different *KIT* cDNA in GIST882-R (data not shown). The same result has been reported by two groups so far [15,31].

For the experimental system used in this study, we generated GIST882-R, a GIST882 cell line with acquired secondary imatinib resistance. In GIST882-R, the expression level of KIT was significantly increased, and autophosphorylation at Y703 was slightly elevated, relative to the parental GIST882 cell line. Previous studies have shown that acquired imatinib-resistant GISTs contain additional mutation(s) in KIT that disrupt imatinib binding, leading to increased autophosphorylation and activation [15]. However, GIST882-R *KIT* mRNA does not contain such additional mutations, but is nonetheless autophosphorylated. This may be attributable, at least in part, to elevated expression of the fully glycosylated membrane-bound KIT in GIST882-R, and/or the presence of other elements involved in the activation of KIT.

3.2. *Enrichment of phosphopeptides and LC-MS/MS-based phosphoproteome analysis of the GIST model system*

In vertebrates, most phosphorylated proteins (phosphoproteins) involved in signal transduction pathways are phosphorylated at Ser/Thr (collectively, 99.95% of phosphoproteins) and/or Tyr residues (0.05%) [32]. The relative scarcity of phospho-Tyr proteins hinders detection of phosphorylated Tyr residues in phosphoproteome analysis. To overcome this difficulty, we utilized two different methods to isolate and concentrate peptides containing phosphorylated Ser, Thr, and/or Tyr residues from the three cell lines of our GIST model system. In the first method (the "titania method"), phosphopeptide-selective titania-based affinity column was used to enrich phosphopeptides containing phosphorylated Ser, Thr, and/or Tyr residues from 25 μg of total protein obtained from each cell line. This method was sufficient to enrich phosphopeptides containing phosphorylated Ser and/or Thr residues. By contrast, the efficiency of the enrichment of phosphopeptides containing phosphorylated Tyr residue was much lower (because of the higher abundance of phosphorylated Ser/Thr over phosphorylated Tyr, as mentioned above). Accordingly, we adopted an alternative

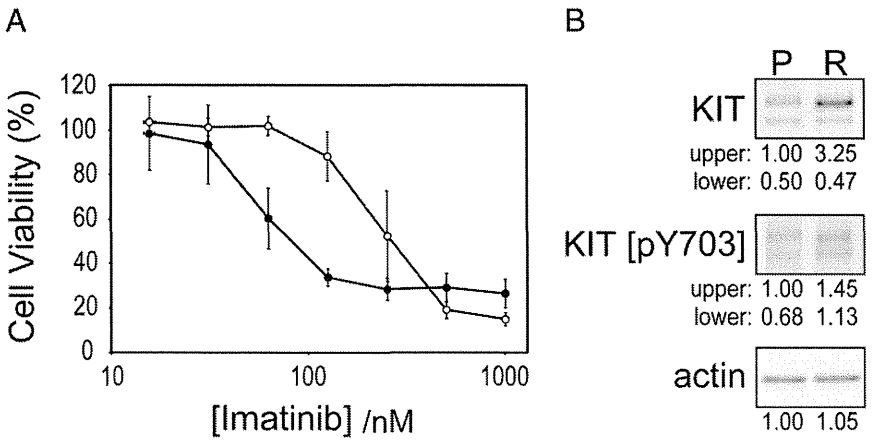

Fig. 1 – Characterization of a secondary imatinib-resistant GIST882 cell line, GIST882-R (A) Results of cell viability assay. Graph shows percentage of cell proliferation relative to untreated cells. The experiment was performed in triplicate and reproduced three times. Open and filled circles indicate the proliferation of GIST882 and GIST882-R, respectively. IC_{50} values were defined as the concentration that inhibited cell proliferation by 50% relative to untreated cells. Bars represent means ± standard deviations (n = 9). Data from GIST882 and GIST882-R were compared using two-tailed Student's t-test (* $p < 0.05$). (B) KIT protein level and phosphorylation of KIT at Y703. Western blotting analysis was performed using anti-KIT and anti-phospho-KIT Y703 antibodies. In addition, the expression level of actin was determined using an anti-actin antibody, as a control protein loading. "P" and "R" indicate GIST882 and GIST882-R, respectively. For each panel, the relative values of band intensity are indicated, which are normalized against the band intensity of "P" (upper band for KIT and KIT [pY703]).

method to specifically enrich phosphotyrosine-containing peptides. In the second method (the "pY-IP method"), we used an anti-phosphotyrosine antibody to perform immunoprecipitations from 3 mg of total protein extracted from each cell line. The combined use of these two different methods for enrichment of phosphopeptides containing phosphorylated Ser, Thr, and/or Tyr residues was critical for our quantitative phosphoproteome analysis, which will be described in subsequent sections.

The phosphopeptides we obtained were subjected to LC-MS/MS analysis, and the resulting peak list was searched against the Swiss-Prot database using the Mascot software. In the titania method, phosphopeptides containing phosphorylated Ser, Thr, and/or Tyr residues that yielded a peptide ion score ≥ 27, the identity threshold ($p < 0.05$), were considered positive identifications. On the other hand, in the pY-IP method, phosphopeptides containing phosphorylated Tyr residues that yielded a peptide ion score ≥ 26 ($p < 0.05$) were considered positive identifications. The differences in the identity thresholds between the titania and pY-IP methods were due to the difference in the number of precursor matches, which was higher for the titania method. Enrichment of the phosphopeptides using the titania method resulted in the identification of 3468 unique phosphopeptides containing phosphorylated Ser, Thr, and/or Tyr residues (three biological replicates from each cell line), whereas enrichment using the pY-IP method resulted in the identification of 472 unique phosphotyrosine-containing peptides (two biological replicates from each cell line). Of these phosphopeptides, 1036 peptides containing phosphorylated Ser, Thr, and/or Tyr residues enriched by the titania method and 210 phosphotyrosine containing peptides enriched by the pY-IP method were determined to be significant by Progenesis LC-MS statistical analysis, and were therefore included in subsequent analyses. The supporting information provides a list of the identified phosphopeptides and their associated quantitative data (Supplementary Tables 1 and 2).

3.3. *Quantitative analysis of the relative abundances of phosphorylation states in KIT and PDGFRA in the three cell lines of the GIST model system*

Mutations of KIT and PDGFRA are associated with GIST formation [33]. Furthermore, as noted above, it is thought that GISTs acquire secondary imatinib resistance predominantly by developing additional mutations in *KIT* [30]; in GIST882-R, however, we detected no additionally mutated *KIT* mRNA. Therefore, we next investigated the possible causes of functional perturbation of KIT and PDGFRA that might be associated with acquisition of imatinib resistance in GIST. To this end, we inspected the phosphorylation sites in KIT and PDGFRA and their associated abundances.

The abundances of phosphopeptides derived from KIT and PDGFRA were determined for 12 and 3 phosphopeptides, respectively (Supplementary Tables 1 and 2). Each of these phosphopeptides corresponds to a different phosphorylation state of KIT (pY609, pY703, pY721, pS746, pY747, pY823, pY900, pY936, pY936/pS943, pS943, pS959, and pS967) or PDGFRA (pY742, pY762, and pY762/pY768). With the exception of pS967 in KIT, these phosphorylation states correspond to data obtained from PhosphoSite (http://www.phosphosite.org/homeAction.do) [34].

Fig. 2A and 2B shows the relative abundance of individual phosphorylation states of KIT and PDGFRA in GIST882, GIST882-IM, and GIST882-R. The profiles of KIT could be categorized into several groups (Fig. 2A (a), (b), and (c)). Phosphorylation of KIT, in many cases, is repressed upon administration of imatinib, but recovers following acquisition of imatinib resistance (Fig. 2A (a) and (b)). On the other hand, phosphorylation at Y936/S943, S943, and S967 of KIT gradually increases as GIST acquires imatinib resistance (Fig. 2A (c)). By contrast, phosphorylation at all identified sites in PDGFRA is repressed upon administration of imatinib, and is repressed further when GIST acquires imatinib resistance (Fig. 2B).

Next, we analyzed the expression level of KIT in each cell line by western blotting. The expression levels of KIT increased in the order GIST882 < GIST882-IM < GIST882-R (Fig. 2C). For reference, the relative abundance of KIT pY703 is also shown by western blotting (Fig. 2C), which increased in the order GIST882-IM < GIST882 < GIST882-R. This result is similar to that of the quantitative LC-MS-based analysis described above (Y703 in Fig. 2A (a)). Collectively, these findings indicated that the expression and phosphorylation levels of KIT are regulated independently.

Among the KIT phosphorylation states that have been detected in quantitative LC-MS analysis, pY703, pY721, pY823, pY900, and pY936 arise via autophosphorylation [35,36]. Other phosphorylation states of KIT, including pY609, pS746, pY747, pS943, pS959, and pS967, are attributed to the activities of other kinases [37]. Collectively, the phosphorylation levels of all the sites listed above were elevated in GIST882-R relative to GIST882-IM.

We next analyzed the expression level of PDGFRA in each cell line by western blotting. The expression level of PDGFRA was higher in GIST882-IM, but almost identical in GIST882-R and GIST882 (Fig. 2C). All of the PDGFRA phosphorylation states that have been detected in quantitative LC-MS analyses (pY742, pY762, and pY768) arise by autophosphorylation. Thus, the kinase activity of PDGFRA was effectively inhibited by imatinib.

As described above, the relative abundances of autophosphorylated states of both KIT and PDGFRA were reduced in GIST882-IM relative to GIST882. However, in GIST882-R, the relative abundances of the autophosphorylated states of KIT and PDGFRA exhibited distinct patterns, with the former being restored and the latter being further reduced. These differences were somewhat surprising because imatinib inhibits the kinase activities of KIT and PDGFRA via the same molecular mechanism, i.e., by occupying the ATP-binding pocket. Importantly, we also identified a novel phosphorylation site of KIT, S967, that has not been reported previously, and analyzed its relative abundance. The functional role of this phosphorylation site remains unknown.

Collectively, our data suggest that the multiplicity of phosphorylation states of KIT and the interconversion between these different states may result in the activation of several signal transduction pathways and/or the development of effective resistance against inhibition of kinase activity by imatinib, leading to acquisition of secondary imatinib resistance in GIST882-R.

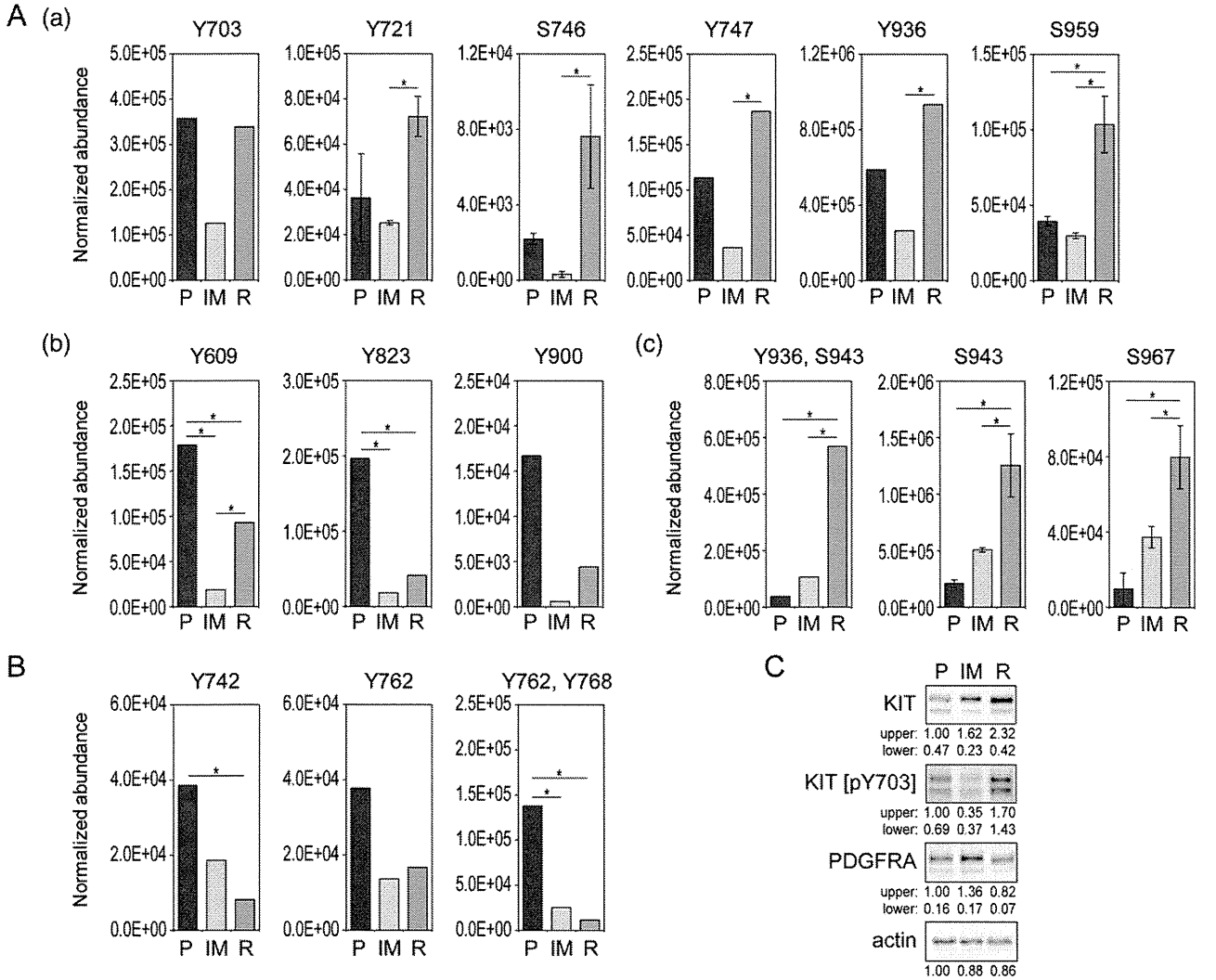

Fig. 2 – Phosphorylation states and expression of KIT and PDGFRA. Graph shows the averaged normalized abundance of 12 and 3 distinct phosphopeptides from KIT (A) and PDGFRA (B), respectively. For phosphopeptides with the same phosphorylation site(s), the peptide with the highest normalized abundance is shown in this figure. The number of amino acids is indicated the phosphorylation site(s). Bars represent means ± standard deviations (n = 3, titania method). Comparison by one-way ANOVA and Tukey's multiple comparison test (* $p < 0.05$). (C) KIT and PDGFRA protein levels and phosphorylation of KIT at Y703 were determined in GIST882, GIST882-IM, and GIST882-R by western blotting. In addition, the expression level of actin was determined using an anti-actin antibody, as a control protein loading. "P", "IM", and "R" indicate GIST882, GIST882-IM, and GIST882-R, respectively. For each panel, the relative values of band intensity are indicated, which are normalized against the band intensity of "P" (upper band for KIT, KIT [pY703], and PDGFRA).

3.4. *Hierarchical clustering and gene ontology analysis*

Next, we subjected the relative abundances for each phosphopeptide of all the proteins identified by the titania and pY-IP methods in GIST882, GIST882-IM, and GIST882-R to hierarchical clustering analysis based on similarity of expression profiles using the Progenesis LC-MS software. GO enrichment analysis by DAVID also allowed us to determine the characterization of each cluster according to the GO term annotations. The dendrograms resulting from hierarchical clustering of phosphopeptides obtained by the titania and pY-IP method are shown in Supplementary Figures 1 and 2, respectively. The phosphopeptides obtained by the titania method (1036 total peptides) were categorized into 7 clusters, and the 210 phosphopeptides obtained by the pY-IP method were categorized into 10 clusters (Supplementary Table 2). Among the categorized clusters, we focused our analysis on two groups of characteristic clusters: (A) cluster 4 from the titania method (Supplementary Figures. 1), and clusters 3 and 7 from the pY-IP method (Supplementary Figures. 2), in which the rank of the values of the standardized normalized abundance was GIST882-R ≈ GIST882 > GIST882-IM; and (B) cluster 2 from the titania method (Supplementary Figures. 1), and clusters 8 and 10 from pY-IP method (Supplementary Figures. 2), in which the rank of the values of the standardized normalized abundance was GIST882-R > GIST882 ≈ GIST882-IM. In GIST882-R as well as GIST882, group (A) consisted of imatinib-unresponsive and constitutive phosphopeptides; by contrast, in GIST882-IM,

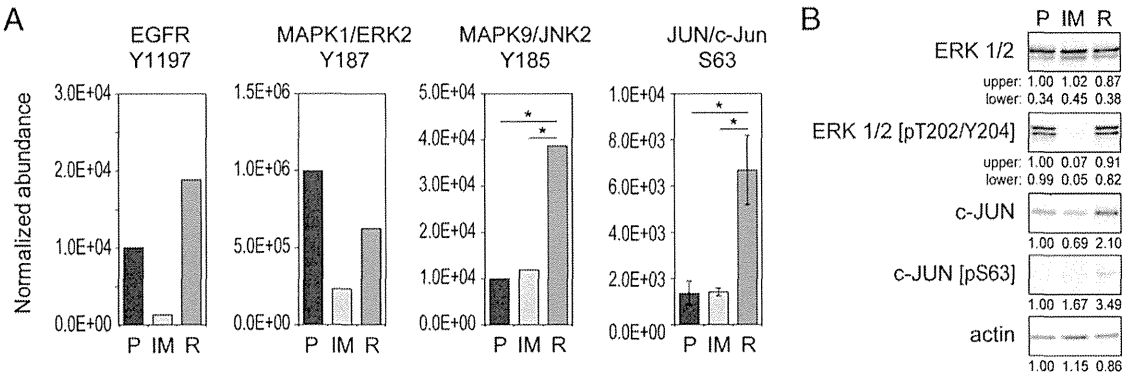

Fig. 3 – Alteration of phosphorylation states in imatinib-resistant cells. (A) Graph shows the averaged normalized abundance of phosphopeptide at Y1197 of EGFR, Y187 of MAPK1/ERK2, Y185 of MAPK9/JNK2, and S63 of JUN/c-Jun. Bars represent means ± standard deviations (n = 3, titania method). Comparison by one-way ANOVA and Tukey's multiple comparison test (* $p < 0.05$). (B) The total expression level and phosphorylation states of ERK1/2 and c-Jun, respectively. Immunoblot analysis was performed using an anti-ERK1/2, anti-phospho-ERK1/2 [T202/Y204], anti-c-Jun, and anti-phospho-c-Jun [S63] antibody. In addition, the expression level of actin was determined using an anti-actin antibody, as a control protein loading. "P", "IM", and "R" indicate GIST882, GIST882-IM, and GIST882-R, respectively. For each panel, the relative values of band intensity are indicated, which are normalized against the band intensity of "P" (upper band for ERK1/2 and ERK1/2 [T202/Y204]).

these phosphopeptides were downregulated in response to imatinib treatment. Group (B) phosphorylated peptides were significantly elevated in GIST882-R relative to GIST882 and GIST882-IM. Thus, we hypothesized that the phosphopeptides in these groups might be closely related to imatinib resistance in GIST882-R.

In group (A), the phosphopeptides were assigned to 128 proteins, including DDR2 (Discoidin domain-containing receptor 2/TKT; Y481), EGFR (Y1197), KIT (Y703, S746, Y747, Y900, and Y936), LYN (tyrosine-protein kinase Lyn; Y194 and Y397), MAPK1 (mitogen-activated protein kinase 1/ERK2; Y187), PTK2 (Focal adhesion kinase 1/FAK; Y576), AKT1S1 (proline-rich Akt1 substrate 1; T246), ARHGAP5 (Rho GTPase-activating protein 5/RhoGAP5; S1173 and S1176), BAD (Bcl2 antagonist of cell death; T80), RRas2 (Ras-related protein R-Ras2; S186), and STAT3 (signal transducer and activator of transcription 3; S727).

GO term annotation analysis of the proteins in group (A) revealed that the cellular component (CC) terms 'plasma membrane' and 'cell projection' were overrepresented in these clusters (Supplementary Table. 3). In addition, the GO term annotations revealed that these proteins were involved in biological processes (BP) such as cell adhesion, regulation of protein kinase activity, positive regulation of cell proliferation, regulation of cellular component movement, and Ras protein signal transduction. EGFR is a transmembrane glycoprotein with an intracellular domain possessing tyrosine kinase activity [38]. Activation of the receptor depends upon the binding of extracellular ligands (EGF and other EGF-like ligands) and dimerization of receptor molecules. EGFR is autophosphorylated, leading to activation of downstream signaling pathways that regulate biological processes such as cell adhesion and proliferation [39]. The phosphopeptide at Y1197 of EGFR, included in cluster 7 of the pY-IP method, was more abundant in GIST882-R than in GIST882 (Fig. 3A). MAPK1/ERK2 is a serine/threonine kinase that functions as an essential component of the ERK cascade, a signaling pathway downstream of RTKs such as KIT and EGFR. Phosphopeptides at Y187 of MAPK1/ERK2 were contained in cluster 3 of the pY-IP method and cluster 4 of the titania method (Fig. 3A). Therefore, these results suggested that reactivation of EGFR and/or KIT, which are RTKs, and subsequent activation of the downstream ERK cascade, might lead to the development of imatinib resistance. Indeed, the increase in normalized abundance of group (A) phosphopeptides in GIST882-R relative to GIST882 and GIST882-IM was similar to the increase in phosphorylated MAPK1/ERK2 level observed by western blotting (Fig. 3B).

In group (B), the phosphopeptides were assigned to 143 proteins including AFAP1L2 (actin filament-associated protein 1-like 2; Y54, Y56, and Y383), CTTN (Src substrate cortactin; Y334), FER (tyrosine-protein kinase Fer; Y402), KIT (Y721, Y936/S943, and S959), LYN (Y473), MAPK9 (mitogen-activated protein kinase 9/JNK2; Y185), SHANK2 (SH3 and multiple ankyrin repeat domains protein 2; Y610), YES1 (tyrosine-protein kinase Yes; Y223), BRAF (serine/threonine-protein kinase B-raf; T401), GRB10 (growth factor receptor–bound protein 10; S428), JUN (transcription factor AP-1/c-Jun; S63), and TNK2 (activated CDC42 kinase 1/ACK1; Y518 and Y827). Furthermore, phosphopeptides from oncoproteins such as BRAF, LYN, JUN, FER, and YES1 were included in these clusters.

GO CC annotations indicated that proteins in group (B) are expressed in the plasma membrane and mitochondrial inner membrane. In addition, GO BP annotations suggested that these proteins are involved in biological processes such as cell surface receptor-linked signal transduction, neurological system processes, and microtubule-based processes (Supplementary Table. 3). JNK, a stress-activated protein kinase that phosphorylates the N-terminus of the transcription factor c-Jun, is involved in many physiological processes including apoptosis. We found that phosphorylation at Y185 and S63 of MAPK9/JNK2 and JUN/c-Jun, respectively, was upregulated in GIST882-R relative to GIST882 and GIST882-IM (Fig. 3A). Immunoblot analysis confirmed that c-Jun phosphorylated at S63 accumulated in the GIST882-R (Fig. 3B). These results

suggested that activation of the JNK cascade might occur in imatinib-resistant cells.

3.5. *Combined administration of inhibitors against KIT and EGFR to GIST882-R results in growth suppression*

Our quantitative phosphoproteome analysis suggested that resistance to imatinib in GIST882-R might result from activation of alternative RTKs, including EGFR, and their downstream signaling pathways. Furthermore, we showed that KIT and EGFR exhibit the same profile of the relative abundances of phosphorylation states among the three cell lines of our GIST model system. Phosphorylation of EGFR was observed only on Y1197, which is in cluster 7 of Supplementary Figures. 2. Here, we chose EGFR to further investigate its role in cell proliferation of GIST882-R cells because it can be inhibited highly specifically. Additionally, advantage of targeting EGFR is the following: (i) it is the most upstream factor of signaling cascade that is activated by autophosphorylation; (ii) specific inhibitor is commercially available; and (iii) its expression in some primary GIST was reported [40,41] but its relation with imatinib resistance was not known.

Fig. 4A shows the relative amounts of EGFR expression in the three cell lines, as determined by western blotting. The total amounts of EGFR were comparable in GIST882 and GIST882-IM, but significantly larger in GIST882-R, similar to the findings for KIT (Section 3.3 and Fig. 2C). Fig. 4B shows the relative total amounts of *EGFR* and *KIT* mRNAs transcribed in the three cell lines, as determined by real-time PCR. The profiles of the total amounts of these mRNAs turned out to be very similar along the three cell lines: comparable in GIST882 and GIST882-IM, but significantly larger in GIST882-R. Thus, the profiles of the expression levels of KIT and EGFR in the three cell lines can be considered to be identical.

Next, in order to investigate the correlation between EGFR activation and proliferation of GIST882-R, we treated this cell line with the anticancer drug gefitinib, which is an inhibitor of EGFR. Fig. 4C shows that the administration of gefitinib alone did not affect the proliferation of GIST882 and GIST882-R, whereas administration of imatinib significantly suppressed the proliferation of GIST882. On the other hand, combined administration of gefitinib and imatinib resulted in partial suppression of the proliferation of GIST882-R: in the presence of imatinib, gefitinib suppressed the proliferation of GIST882-R in a dose-dependent manner. In the previous reports, it was shown that both imatinib [24] and gefitinib induce apoptosis [42], and thereby, we assume that combined use of these drugs results in apoptosis in GIST882-R cells. As far as we know, there is no report showing that EGFR contributes to the prognosis of GIST progression, and thus this is the first report suggesting that EGFR is relevant to this event. These results suggested that suppression of cell proliferation signals in secondary imatinib-resistant GIST882-R cells requires simultaneous inhibition of multiple kinase activities.

4. Conclusions

Our proteome-wide phosphorylation analysis of a cell-based GIST model revealed a close correlation between the secondary imatinib resistance of GISTs and activation of signal transduction, accompanied by upregulation of RTKs such as KIT and EGFR. Further investigations identified the RTKs as potential targets for suppression of the cell proliferation of imatinib-resistant GIST cells, suggesting a clinical approach for use in patients with imatinib-resistant GIST.

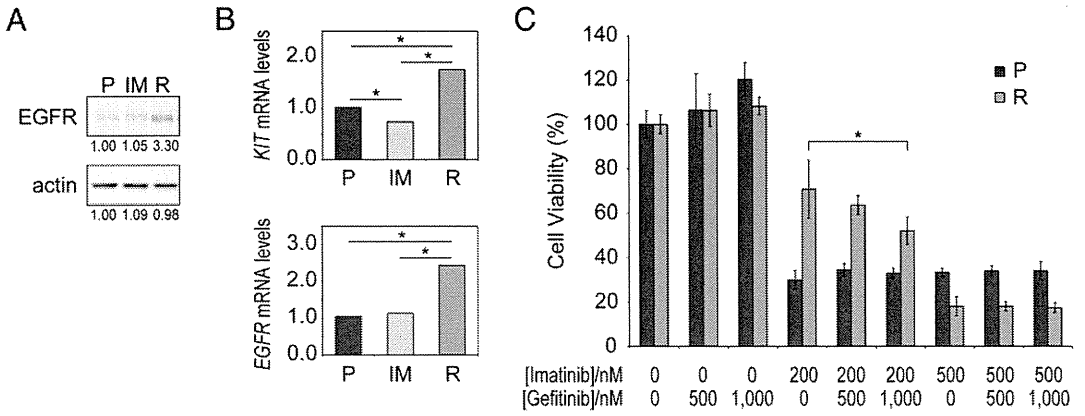

Fig. 4 – Alteration of phosphorylation states in imatinib-resistant cells. (A) EGFR protein level was determined by western blotting in GIST882, GIST882-IM, and GIST882-R. Also, the expression level of actin was investigated using anti-actin antibody as a control for the amount of protein loaded. For each panel, the relative values of band intensity are indicated, which are normalized against the band intensity of "P". (B) The total mRNA levels of *KIT* and *EGFR* were determined by qRT-PCR. All mRNA levels were normalized to *GAPDH*. Comparisons were performed by one-way ANOVA and Tukey's multiple comparison test (* $p < 0.05$). (C) The effect of combined treatment with two inhibitors on proliferation. Graph shows percentage of cell proliferation relative to untreated cells. Bars represent means ± standard deviations ($n = 6$). The two data sets were compared using two-tailed Student's *t*-test (* $p < 0.05$). "P", "IM", and "R" indicate GIST882, GIST882-IM, and GIST882-R, respectively.

5. Conflict of interest

The authors declare that no conflict of interest exists.

Acknowledgments

The authors thank Dr. Jonathan A. Fletcher (Brigham and Women's Hospital, Boston, USA) for providing the GIST882 cell line. This work was supported by the Special Coordination Fund for Promoting Science and Technology, "Creation and Innovation Centers for Advanced Interdisciplinary Research Areas" (11800122).

Appendix A. Supplementary data

Supplementary data to this article can be found online at http://dx.doi.org/10.1016/j.jprot.2014.12.012.

REFERENCES

[1] Hirota S, Isozaki K, Moriyama Y, Hashimoto K, Nishida T, Ishiguro S, et al. Gain-of-function mutations of c-kit in human gastrointestinal stromal tumors. Science 1998;279:577–80.
[2] Kindblom LG, Remotti HE, Aldenborg F, Meis-Kindblom JM. Gastrointestinal pacemaker cell tumor (GIPACT): gastrointestinal stromal tumors show phenotypic characteristics of the interstitial cells of Cajal. Am J Pathol 1998;152:1259–69.
[3] Sircar K, Hewlett BR, Huizinga JD, Chorneyko K, Berezin I, Riddell RH. Interstitial cells of Cajal as precursors of gastrointestinal stromal tumors. Am J Surg Pathol 1999;23:377–89.
[4] Rubin BP, Heinrich MC, Corless CL. Gastrointestinal stromal tumour. Lancet 2007;369:1731–41.
[5] Corless CL, Schroeder A, Griffith D, Town A, McGreevey L, Harrell P, et al. PDGFRA mutations in gastrointestinal stromal tumors: frequency, spectrum and in vitro sensitivity to imatinib. J Clin Oncol Off J Am Soc Clin Oncol 2005;23:5357–64.
[6] Heinrich MC, Corless CL, Duensing A, McGreevey L, Chen CJ, Joseph N, et al. PDGFRA activating mutations in gastrointestinal stromal tumors. Science 2003;299:708–10.
[7] Duensing A, Medeiros F, McConarty B, Joseph NE, Panigrahy D, Singer S, et al. Mechanisms of oncogenic KIT signal transduction in primary gastrointestinal stromal tumors (GISTs). Oncogene 2004;23:3999–4006.
[8] Joensuu H, Hohenberger P, Corless CL. Gastrointestinal stromal tumour. Lancet 2013;382:973–83.
[9] Corless CL, Fletcher JA, Heinrich MC. Biology of gastrointestinal stromal tumors. J Clin Oncol Off J Am Soc Clin Oncol 2004;22:3813–25.
[10] Dematteo RP, Heinrich MC, El-Rifai WM, Demetri G. Clinical management of gastrointestinal stromal tumors: before and after STI-571. Hum Pathol 2002;33:466–77.
[11] Buchdunger E, Zimmermann J, Mett H, Meyer T, Muller M, Druker BJ, et al. Inhibition of the Abl protein-tyrosine kinase in vitro and in vivo by a 2-phenylaminopyrimidine derivative. Cancer Res 1996;56:100–4.
[12] van Oosterom AT, Judson I, Verweij J, Stroobants S, Donato di Paola E, Dimitrijevic S, et al. Safety and efficacy of imatinib (STI571) in metastatic gastrointestinal stromal tumours: a phase I study. Lancet 2001;358:1421–3.
[13] Demetri GD, von Mehren M, Blanke CD, Van den Abbeele AD, Eisenberg B, Roberts PJ, et al. Efficacy and safety of imatinib mesylate in advanced gastrointestinal stromal tumors. N Engl J Med 2002;347:472–80.
[14] Pierotti MA, Tamborini E, Negri T, Pricl S, Pilotti S. Targeted therapy in GIST: in silico modeling for prediction of resistance. Nat Rev Clin Oncol 2011;8:161–70.
[15] Nishida T, Kanda T, Nishitani A, Takahashi T, Nakajima K, Ishikawa T, et al. Secondary mutations in the kinase domain of the KIT gene are predominant in imatinib-resistant gastrointestinal stromal tumor. Cancer Sci 2008;99:799–804.
[16] Stasyk T, Huber LA. Mapping in vivo signal transduction defects by phosphoproteomics. Trends Mol Med 2012;18:43–51.
[17] Schmelzle K, White FM. Phosphoproteomic approaches to elucidate cellular signaling networks. Curr Opin Biotechnol 2006;17:406–14.
[18] Kearney M, Palmer S, Maldarelli F, Shao W, Polis MA, Mican J, et al. Frequent polymorphism at drug resistance sites in HIV-1 protease and reverse transcriptase. Aids 2008;22:497–501.
[19] Rappsilber J, Ishihama Y, Mann M. Stop and go extraction tips for matrix-assisted laser desorption/ionization, nanoelectrospray, and LC/MS sample pretreatment in proteomics. Anal Chem 2003;75:663–70.
[20] Sugiyama N, Masuda T, Shinoda K, Nakamura A, Tomita M, Ishihama Y. Phosphopeptide enrichment by aliphatic hydroxy acid-modified metal oxide chromatography for nano-LC-MS/MS in proteomics applications. Mol Cell Proteomics 2007;6:1103–9.
[21] Rush J, Moritz A, Lee KA, Guo A, Goss VL, Spek EJ, et al. Immunoaffinity profiling of tyrosine phosphorylation in cancer cells. Nat Biotechnol 2005;23:94–101.
[22] Huang DW, Sherman BT, Lempicki RA. Bioinformatics enrichment tools: paths toward the comprehensive functional analysis of large gene lists. Nucleic Acids Res 2008;37:1–13.
[23] Botstein D, Cherry JM, Ashburner M, Ball CA, Blake JA, Butler H, et al. Gene Ontology: tool for the unification of biology. Nat Genet 2000;25:25–9.
[24] Tuveson DA, Willis NA, Jacks T, Griffin JD, Singer S, Fletcher CD, et al. STI571 inactivation of the gastrointestinal stromal tumor c-KIT oncoprotein: biological and clinical implications. Oncogene 2001;20:5054–8.
[25] Longley Jr BJ, Metcalfe DD, Tharp M, Wang X, Tyrrell L, Lu SZ, et al. Activating and dominant inactivating c-KIT catalytic domain mutations in distinct clinical forms of human mastocytosis. Proc Natl Acad Sci U S A 1999;96:1609–14.
[26] Bougherara H, Subra F, Crepin R, Tauc P, Auclair C, Poul MA. The aberrant localization of oncogenic kit tyrosine kinase receptor mutants is reversed on specific inhibitory treatment. Mol Cancer Res 2009;7:1525–33.
[27] Xiang Z, Kreisel F, Cain J, Colson A, Tomasson MH. Neoplasia driven by mutant c-KIT is mediated by intracellular, not plasma membrane. Recept Signal Mol Cell Biol 2006;27:267–82.
[28] Prenen H, Stefan C, Landuyt B, Vermaelen P, Debiec-Rychter M, Bollen M, et al. Imatinib mesylate inhibits glucose uptake in gastrointestinal stromal tumor cells by downregulation of the glucose transporters recruitment to the plasma membrane. Am J Biochem Biotechnol 2005;1:95–102.
[29] Sun J, Pedersen M, Bengtsson S, Ronnstrand L. Grb2 mediates negative regulation of stem cell factor receptor/c-kit signaling by recruitment of Cbl. Exp Cell Res 2007;313:3935–42.
[30] Gounder MM, Maki RG. Molecular basis for primary and secondary tyrosine kinase inhibitor resistance in gastrointestinal stromal tumor. Cancer Chemother Pharmacol 2011;67(Suppl. 1):S25–43.
[31] Lim KH, Huang MJ, Chen LT, Wang TE, Liu CL, Chang CS, et al. Molecular analysis of secondary kinase mutations in imatinib-resistant gastrointestinal stromal tumors. Med Oncol 2007;25:207–13.

[32] Bergstrom Lind S, Molin M, Savitski MM, Emilsson L, Astrom J, Hedberg L, et al. Immunoaffinity enrichments followed by mass spectrometric detection for studying global protein tyrosine phosphorylation. J Proteome Res 2008;7:2897–910.
[33] Isozaki K, Hirota S. Gain-of-function mutations of receptor tyrosine kinases in gastrointestinal stromal tumors. Curr Genomics 2006;7:469–75.
[34] Hornbeck PV, Kornhauser JM, Tkachev S, Zhang B, Skrzypek E, Murray B, et al. PhosphoSitePlus: a comprehensive resource for investigating the structure and function of experimentally determined post-translational modifications in man and mouse. Nucleic Acids Res 2011;40:D261–70.
[35] Thommes K, Lennartsson J, Carlberg M, Ronnstrand L. Identification of Tyr-703 and Tyr-936 as the primary association sites for Grb2 and Grb7 in the c-Kit/stem cell factor receptor. Biochem J 1999;341:211–6.
[36] DiNitto JP, Deshmukh GD, Zhang Y, Jacques SL, Coli R, Worrall JW, et al. Function of activation loop tyrosine phosphorylation in the mechanism of c-Kit auto-activation and its implication in sunitinib resistance. J Biochem 2010;147:601–9.
[37] Ronnstrand L. Signal transduction via the stem cell factor receptor/c-Kit. Cell Mol Life Sci 2004;61:2535–48.
[38] Bethune G, Bethune D, Ridgway N, Xu Z. Epidermal growth factor receptor (EGFR) in lung cancer: an overview and update. J Thorac Dis 2010;2:48–51.
[39] Andl CD, Mizushima T, Nakagawa H, Oyama K, Harada H, Chruma K, et al. Epidermal growth factor receptor mediates increased cell proliferation, migration, and aggregation in esophageal keratinocytes in vitro and in vivo. J Biol Chem 2002;278:1824–30.
[40] Qiu X, Montgomery E. Expression of EGFR in gastric stromal tumors: a clinicopathologic study. Appl Immunohistochem Mol Morphol 2008;16:310–5.
[41] Nakagawa M, Nabeshima K, Asano S, Hamasaki M, Uesugi N, Tani H, et al. Up-regulated expression of ADAM17 in gastrointestinal stromal tumors: coexpression with EGFR and EGFR ligands. Cancer Sci 2009;100:654–62.
[42] Ciardiello F, Caputo R, Bianco R, Damiano V, Pomatico G, De Placido S, et al. Antitumor effect and potentiation of cytotoxic drugs activity in human cancer cells by ZD-1839 (Iressa), an epidermal growth factor receptor-selective tyrosine kinase inhibitor. Clin Cancer Res 2000;6:2053–63.